

Article

Secondary Organic Aerosol (SOA) from Photo-Oxidation of Toluene: 1 Influence of Reactive Nitrogen, Acidity and Water Vapours on Optical Properties

Kalyan Mitra ¹, Harsh Raj Mishra ², Xiangyu Pei ^{1,†} and Ravi Kant Pathak ^{1,*}

¹ Department of Chemistry and Molecular Biology, University of Gothenburg, SE-41296 Gothenburg, Sweden; kalyan.mitra@gu.se (K.M.); xiangyupei@zju.edu.cn (X.P.)

² Indo Gangetic Plains—Center for Air Research and Education (IGP—CARE), Hamirpur U.P. 210501, India; mishraharshraj800@gmail.com

* Correspondence: ravikant@chem.gu.se

† Current address: College of Environmental and Resource Sciences, Zhejiang University, Hangzhou 31005, China.

Abstract: Many climate models treat the light-absorbing SOA component called “brown carbon” (BrC) as non-light absorbing because its formation and transformations are poorly understood. We therefore investigated the influence of reactive nitrogen (NO_x , NH_3)-, acidity (H_2SO_4)-, and water-mediated chemistry on SOA formed by the photo-oxidation of toluene, the subsequent formation and transformation of BrC, and its optical properties. We discovered that nitrogen-poor (NP) SOA is formed when the molar ratio of NO_x to reacted toluene (henceforth, $[\text{NO}_x/\Delta\text{HHC}]$) is 0.15 or less, whereas nitrogen-rich (NR) SOA is formed when $[\text{NO}_x/\Delta\text{HHC}] > 0.15$. NR and NP SOA have markedly different characteristics. The light absorption coefficient (B_{abs}) and mass absorption cross-section (MAC) of the SOA increased with $[\text{NO}_x/\Delta\text{HHC}]$ under both the NP and NR regimes. For NP SOA, the MAC increased with $[\text{NO}_x/\Delta\text{HHC}]$ independently of the relative humidity (RH). However, the MAC of NR SOA was RH-dependent. Under both NP and NR regimes, acidity promoted SOA browning while NH_3 increased B_{abs} and MAC at 80% RH. The highest MAC was observed at the lowest RH (20%) for acidic NR SOA, and it was postulated that the MAC of SOA depends mainly on the pH and the $[\text{H}^+]_{\text{free}}/[\text{SOA mass}]$ ratio of the aqueous SOA phase.

Keywords: switching optical property; photo-oxidation; secondary organic aerosol (SOA); NO_x ramping; nitrogen-poor (NP); nitrogen-rich (NR); toluene; sulfuric acid; ammonia ramping



Citation: Mitra, K.; Mishra, H.R.; Pei, X.; Pathak, R.K. Secondary Organic Aerosol (SOA) from Photo-Oxidation of Toluene: 1 Influence of Reactive Nitrogen, Acidity and Water Vapours on Optical Properties. *Atmosphere* **2022**, *13*, 1099. <https://doi.org/10.3390/atmos13071099>

Academic Editor: Akinori Ito

Received: 31 May 2022

Accepted: 30 June 2022

Published: 13 July 2022

Publisher's Note: MDPI stays neutral with regard to jurisdictional claims in published maps and institutional affiliations.



Copyright: © 2022 by the authors. Licensee MDPI, Basel, Switzerland. This article is an open access article distributed under the terms and conditions of the Creative Commons Attribution (CC BY) license (<https://creativecommons.org/licenses/by/4.0/>).

1. Introduction

Atmospheric aerosols markedly affect the radiative balance in the Earth's atmosphere and play key roles in climatic processes [1]. Carbonaceous aerosols consisting of organic carbon (OC) and black carbon (BC, commonly known as “soot”) comprise a major fraction of atmospheric aerosols [2,3]. Soot warms the planet because it strongly absorbs light, but most climate models have traditionally treated OC as a light-scattering (and thus cooling) substance [1]. The cooling due to this scattering partly offsets the warming caused by BC co-emitted during combustion processes [4]. The molecular composition of OC and its evolution during various atmospheric aging processes have been studied extensively in recent decades [2,3,5–9]. However, despite various advances, our understanding of the climate-related properties of atmospheric OC and its effects on the atmospheric environment and climate forcing remains incomplete. In particular, we need to better understand the behaviour of the OC fraction in various strongly light-absorbing complex mixing states that are collectively known as Brown Carbon (BrC). OC can be emitted directly through combustion processes that form so-called primary organic aerosol (POA) or formed in the atmosphere by gas-to-particle conversion processes that generate secondary organic

aerosol (SOA). The latter processes include nucleation, condensation, and heterogeneous and multiphase chemical reactions that form highly oxidized multifunctional molecules (HOMs) with extremely low volatility and high molecular weights [3,10,11], some of which are strongly light-absorbing [12–15].

Known primary and secondary sources of BrC aerosols include fossil fuel combustion [16], biomass burning [17,18], biological aerosols (e.g., soil humics and bioaerosols) [19], and SOA formed from anthropogenic or biogenic precursors [13]. While the primary BrC sources are straightforward to identify, the mechanisms that generate light-absorbing SOA are largely unknown [8]. Quantifying BrC's contribution to light absorption is critically important for accurate interpretation of the aerosol optical depth (AOD), i.e., the light extinction within the atmospheric column due to scattering and absorption.

Aromatic compounds comprise 20–40% of gasoline by volume and are major anthropogenic volatile organic compounds (VOCs) that play an important role in the formation of tropospheric ozone and SOA [20–23]. The aromatic compounds toluene and benzene are thought to be some of the most important SOA precursors because of their high anthropogenic emissions and SOA formation potential [20,22,24–28]. The optical properties of aromatic-derived SOA have therefore been studied extensively over the last decade [26–34]. The highest mass absorption coefficient (MAC) values are observed for toluene SOA formed under high-NO_x conditions at moderate RH with short photolysis aging times [27]. However, the optical properties of toluene/benzene-derived SOA formed under other atmospherically-relevant conditions are unclear. In particular, there are four major factors whose effects on the light absorption characteristics of toluene SOA are unknown: (1) the molar ratio of NO_x to reacted toluene ([NO_x/ΔH_C] in the atmosphere, (2) the RH and the dependence of its effects on [NO_x/ΔH_C], (3) acidity and the dependence of its effects on [NO_x/ΔH_C] and the RH, and (4) aging in the presence of [OH]. Determining the effects of these factors will greatly improve our understanding of a complex and important air pollution component by explaining how NH₃, water, NO_x, and acidity affect the formation and transformation of secondary BrC (SBrC).

To holistically assess the environmental effects of BrC, a deep understanding of its optical properties and the relationships between SOA formation processes under diverse atmospheric pollution scenarios is required. This study therefore investigates the light absorption characteristics of laboratory-generated SOA under simulated urban environmental conditions. Toluene was chosen as an SOA precursor representative of anthropogenic emissions. A matrix of experiments was conducted to determine the effects of (1) NO_x, (2) water, (3) NH₃, and (4) acidity on the mass of SOA that is formed and its light absorption and scattering characteristics. It is shown that reactive nitrogen, acidity, and water all influence SOA browning and that the SOA formed during toluene photooxidation may be either nitrogen-poor (NP) or nitrogen-rich (NR). These results provide a base for (i) developing improved parametrizations to describe radiative forcing due to toluene SOA for climate models and (ii) evaluating models against field observations under various atmospheric pollution scenarios.

2. Materials and Methods

2.1. Experiments

2.1.1. Experimental Setup

The experiment was designed to generate SOA with tight control over experimental parameters and to measure and record changes in its formation, transformation, and properties under diverse experimental conditions. As shown in Figure S1 of the Supplementary Information (henceforth referred to as “Supplementary Materials”), the experimental set-up consisted of three serial zones: (i) the reactants input control zone, (ii) the reaction zone, and (iii) the instrumentation and measurement zone. The reactants input control zone regulated the flows and concentrations of gases and aerosols in the reaction zone. In the reaction zone, photo-induced reactions leading to SOA formation and transformation were allowed to occur subject to tightly controlled time constraints. In the instrumentation and

measurement zone, various parameters, concentrations, and properties of the gas and aerosol mixture at the outflow of the reaction zone were measured and recorded.

The Gothenburg Potential Aerosol Mass chamber (Go:PAM) was used as the photo-oxidation reaction zone [35]. This apparatus is depicted schematically in Figure S1 OH radicals are produced in Go:PAM by photolyzing O₃ in the presence of water vapour. Total flows through the apparatus were measured, revealing that the reactants had a median residence time of 100 s and SOA was formed in a laminar flow. The main inputs in the reactant input control zone were toluene (VOC), water vapour, and O₃. NO_x, NH₃, and H₂SO₄ were also added in some experiments as described below. To check *the accelerated aging in lab environment with 100 s median residence time*, the Toluene & O₃ was taken in higher quantities than atmospherically-relevant conditions. Most of the experiments used ramping NO_x concentrations but some used an NH₃ ramp. If a given input was not used in an experiment, the pipe connecting that input to the Go:PAM chamber was blocked to ensure that only the desired reactants were admitted. VOC-free air was generated with a Zero-Air generator. O₃ was generated by photolyzing VOC-free air with UVP Pen-Ray®mercury lamps (185 nm) and allowed to flow into the Go:PAM chamber. The desired RH in the Go:PAM chamber was set using an RH generator consisting of a water bubbler maintained at a user-specified temperature; VOC-free air was used to carry the required amount of moisture into the Go:PAM chamber. Similarly, to establish the desired VOC concentration in the Go:PAM chamber, VOC-free air was passed through a VOC container (which was heated to a user-specified temperature below the VOC's boiling point using a water bath) to carry the VOC into Go:PAM chamber. H₂SO₄ seeds were generated from an H₂SO₄ solution using the TSI Atomizer flow with VOC-free air; the flow was controlled with a needle valve that allowed a majority of the H₂SO₄ to be sent to the exhaust with a small seed fraction being dried with a silicon drier and sent to the Go:PAM chamber. The required flow through the FIGAERO-HR-ToF-CIMS instrument during gas phase sampling differed from that for particle phase sampling. Therefore, VOC-free Air was used to dilute the FIGAERO-HR-ToF-CIMS flow to enable control over the flow through the instrument.

In the instrumentation and measurement zone, a SMPS (CPC 3775; EC3080 TSI Inc. Shoreview, MN, USA) was used to measure the particle number concentration and volume concentration of SOA in the sample outflow. The absorption and scattering properties of the SOA were measured with a 3-wavelength photoacoustic soot spectrometer (PASS-3) after passage through a charcoal filter to remove residual VOCs and NO_x. Both instruments were described previously by Backstrom, D., et al. [36] and were used under the experimental conditions specified in Table 1. Gas- and aerosol-phase oxidation products were measured with the Filter Inlet for Gases and AEROSols (FIGAERO) instrument of Aerodyne Research Inc., Billerica, MA, USA [37] and by high-resolution chemical ionization mass spectrometry (ToF-CIMS, Aerodyne Research Inc. and Tofwerk AG, Thun, Switzerland) [38]. The reagent ion for CI detection was I⁻. Additionally, an O₃ monitor, a VOC monitor (photoionization technique using model: PID AH2, from ALPHASENSE LIMITED, Reg. no. 03264282, Essex, UK), an RH monitor, and a temperature monitor were used to measure the properties of the residual flow after passing through the Go:PAM Chamber. The NO_x concentration (consisting of equal quantities of NO and NO₂) was ramped from 61 ppb to 361 ppb, while that of NH₃ was ramped from 42 to 203 ppb.

Table 1. The experimental input matrix.

Exp.ID	Reacted Toluene (Δ H C) Concentration (ppb) [§]	NO _x (NO:NO ₂ Ratio = 1:1) Range (Initial to Final, ppb)	O ₃ (Initial, ppb)	RH%	NH ₃ Ramp	H ₂ SO ₄ (μ g m ⁻³)	OH _{expo} (Calculated) $\times 10^{11}$ (cm ⁻³ ·s)	Remarks
Tol-1	1161	31 to 362	999	80	No	No	2.8	NO _x ramped
Tol-2	1064	31 to 362	999	65	No	No	2.3	NO _x ramped
Tol-3	870	31 to 362	999	35	No	No	1.6	NO _x ramped
Tol-4	774	31 to 362	999	20	No	No	1.3	NO _x ramped
Tol-5	1161	61	999	80	Yes	No	2.8	NH ₃ Ramp. NO _x constant
Tol-6	1161	360	999	80	Yes	No	2.8	NH ₃ Ramp. NO _x constant
Tol-7	1161	30 to 351	999	80	No	Yes (22.3)	2.8	NO _x ramped
Tol-8	1161	30 to 351	999	65	No	Yes (22.3)	2.8	NO _x ramped
Tol-9	780	30 to 351	999	20	No	Yes (22.3)	1.6	NO _x ramped

[§]: Toluene reacted is calculated by measuring residual toluene from Go:PAM outlet with a VOC monitor with and without reaction at Go:PAM.

2.1.2. OH Radical Generation

The main oxidant of toluene in our experiments was OH generated by O₃ photolysis in the presence of water vapor in GO:PAM. O₃ was generated by external irradiation of VOC-free air with a mercury lamp ($\lambda = 185$ nm) and its concentration was measured with an O₃ monitor (2B Technologies, Boulder, CO, USA). UV photolysis of O₃ ($\lambda = 254$ nm) generated excited oxygen [O(₁D)] atoms inside the flow tube (Go:PAM) at a relative humidity of 20–80%. It was previously established that Go:PAM OH exposures can be determined by measuring the residual VOC concentration at the outlet of Go:PAM with a VOC monitor [39,40]. In this study, the OH radical exposure and concentrations were estimated using Equation (3). Assuming an average atmospheric OH concentration of 1.5×10^6 molecules cm⁻³ [41], our experimental conditions correspond to about 0.77 to 1.61 days of atmospheric oxidation aging (See Table S1 in Supplementary Materials).

2.1.3. Experimental Matrix

The experiments performed in this study are summarized in Table 1. Controlled experimental variables included the toluene concentration (Δ H C), the initial ozone concentration, the relative humidity, the NO_x ramp and initial concentration (31 ppb to 362 ppb for experiments Tol-1 to Tol-4 and 30 ppb to 351 ppb for experiments Tol-7 to Tol-9), and the NH₃ ramp (42 ppb to 203 ppb for experiments Tol-5 and Tol-6). The results of these experiments are summarized in Table 2. This table includes the experiment ID and the average mass of SOA formed under NP ($[\text{NO}_x]/[\Delta\text{H C}] \leq 0.15$) and NR ($[\text{NO}_x]/[\Delta\text{H C}] > 0.15$) conditions as well as the average values of the aerosol absorption coefficient (B_{abs} [Mm⁻¹]), the aerosol scattering coefficient (B_{scat} [Mm⁻¹]) at 405 nm and 781 nm, the mass absorption cross-section (MAC [m² g⁻¹]), the single scattering albedo (SSA), and the mass scattering cross-section (MSC [m²g⁻¹]) for NP and NR SOA at 405 nm, together with the calculated

OH concentration and estimated aging of SOA in days. The observations made during the experiments and rationales for their outcomes are discussed in Section 3.

Table 2. Summary of experimental results.

Exp. ID	SOA Type	SOA Mass $\mu\text{g m}^{-3}$	$B_{\text{abs},405}$ Mm^{-1}	$B_{\text{abs},781}$ Mm^{-1}	$B_{\text{scat},405}$ Mm^{-1}	$B_{\text{scat},781}$ Mm^{-1}	MAC_{405} m^2g^{-1}	MSC_{405} m^2g^{-1}	OH (Molecules $\text{cm}^{-3}\cdot\text{s} \times 10^{11}$; [SOA Aging in Days])	Average Mobility Diameter (nm)
Tol-1	NP	552	11.8	0.320	1259	66.5	0.021	2.29	2.8; [1.61]	65.0
	NR	520	25.2	0.112	1258	67.4	0.048	2.38		64.7
Tol-2	NP	372	8.15	0.000	805	39.1	0.022	2.13	2.3; [1.33]	60.8
	NR	358	14.5	0.000	788	38.3	0.040	2.20		62.8
Tol-3	NP	261	5.31	0.937	516	22.3	0.020	1.88	1.6; [0.93]	58.8
	NR	223	10.3	0.195	451	20.3	0.045	1.95		57.7
Tol-4	NP	162	3.73	0.000	318	14.0	0.024	2.05	1.3; [0.77]	57.0
	NR	134	6.10	0.042	258	11.4	0.041	1.77		55.0
Tol-5	NP	465	13.3	0.246	2958	285.8	0.029	6.39	2.8; [1.61]	94.6
Tol-6	NR	432	40.1	0.025	1500	0.000	0.093	3.48	2.8; [1.61]	64.5
Tol-7	NP	375	11.5	0.000	1582	113.8	0.030	4.19	2.8; [1.61]	63.9
	NR	416	25.6	0.626	1950	139.6	0.061	4.57		64.5
Tol-8	NP	348	12.4	0.085	1747	127.4	0.035	5.05	2.8; [1.61]	91.2
	NR	321	21.4	0.987	1632	117.9	0.068	5.06		89.3
Tol-9	NP	192	7.86	0.000	807	55.2	0.041	4.14	1.6; [0.93]	87.8
	NR	182	10.3	0.000	738	51.4	0.058	4.05		88.1

The NO_x concentration was ramped at a relatively slow rate of 1 ppb NO_x /min so changes in its concentration and flow were not drastic. All of the experiments involved periodic flow changes at 30 min intervals because the FIGAERO-HR-ToF-CIMS instrument alternates between gas phase and particle phase sampling modes roughly every 30 min. The exhaust flow of the Go:PAM system was diluted with VOC-free air at a flow rate of 3 L per min with an MFC to manage the fluctuating requirements of the FIGAERO-HR-ToF-CIMS. The FIGAERO-HR-ToF-CIMS extracted 4 L per minute for gas phase measurements when operating in particle collection mode but only 2 L per minute while analysing the previously collected particle phase samples.

2.2. Methods

2.2.1. Data Processing

All results obtained using the SMPS and PASS3 instruments as well as the acidity values and concentrations of NO_x and NH_3 presented in this work are averages of measurements conducted over periods of around 30 min. Molecular speciation of toluene SOA was performed by analysing gas and aerosol samples drawn from the GO:PAM flow tube outlet at a rate of 4 L per minute by the FIGAERO-HR-ToF-CIMS, operating in particle collection mode. The FIGAERO-HR-ToF-CIMS operated in this mode in 30-min intervals; results obtained using other instruments when the FIGAERO-HR-ToF-CIMS was not operating in particle collection mode were discarded. Also excluded from the analysis were measurements of the SOA mass and bulk properties obtained in cases where the NO_x concentration was initially very low or negligible, for example because the NO_x ramp MFC valve failed to open.

2.2.2. Calculations

The toluene SOA mass was estimated using the previously reported densities of toluene SOA formed under low (1.24 g cm^{-3}) and high (1.45 g cm^{-3}) NO_x conditions [20].

The absorption coefficient B_{abs} and B_{scat} were calculated [42] as described in the operator's manual of the PASS3 instrument.

The *Mass Absorption Coefficient (MAC)* of toluene SOA at a given wavelength λ , MAC_{λ} , was calculated as

$$MAC_{\lambda} = B_{\text{abs(toluene SOA. } \lambda)} / \text{toluene SOA mass} \quad (1)$$

The *Mass Scattering Coefficient (MSC)* of toluene SOA at a given wavelength λ , MSC_{λ} , was calculated as

$$MSC_{\lambda} = B_{\text{scat(toluene SOA. } \lambda)} / \text{toluene SOA mass} \quad (2)$$

The total OH concentration exposure (OH_{expo}) under various experimental conditions was estimated using Equation (3) from the initial and final toluene concentrations in the flow reactor (Go: PAM) and the reaction constant (K_{OH}) for the reaction between the OH radical and toluene [43] using Equation (3). The equivalent atmospheric aging was estimated in hours and days as $OH_{\text{expo}}/3600$ and $OH_{\text{expo}}/86,400$, respectively, as shown in Table S1 (See Supplementary Materials).

$$OH_{\text{expo}} = \frac{-\ln\left(\frac{\text{Toluene}_{\text{final}}}{\text{Toluene}_{\text{initial}}}\right)}{K_{\text{OH}}} \quad (3)$$

2.2.3. Models

We used the Extended AIM Aerosol Thermodynamics Model [44] to estimate the aerosol water content in the H_2SO_4 seeds at various RH and the free H^+ ion concentration in the aerosol phase. E-AIM is a community model for calculating gas/liquid/solid partitioning in aerosol systems containing inorganic and organic components and water, and solute and solvent activities in aqueous solutions and liquid mixtures. We used Model I under the assumption that the H_2SO_4 seeds in our experiments would have instantaneously absorbed water before the SOA condensed on them during the toluene-OH oxidation and condensation process. These calculations were used to estimate the pH of the aerosol mixture of H_2SO_4 coated with SOA.

3. Results and Discussion

3.1. Summary of Key Experimental Results

The mass of SOA formed at $[NO_x]/[\Delta HC]$ molar ratios below 0.15 was substantially greater than at higher $[NO_x]/[\Delta HC]$ values. Previous studies attributed the reduced SOA mass at higher NO_x concentrations to the formation of nitrogen-rich SOA compounds such as organo-nitrates, which are relatively volatile and thus have a strong tendency to partition into the gas phase [45,46]. We therefore analyse the nitrogen-poor (NP) and nitrogen-rich (NR) SOA formation regimes separately.

The main experimental results obtained in this work are summarized in Table 2. It should be noted that the initial toluene and O_3 concentration and the UV light intensity were the same in all experiments. However, the amount of toluene reacted (ΔHC) differed between experiments, especially in experiments Tol-1 to Tol-4, where RH was the only quantity that varied. This difference in ΔHC can be attributed to the variation in RH, which was found to be strongly and positively correlated with ΔHC (See Figure S1). The absorption of the 781 nm laser light by both SOA types was negligible (i.e., within the noise range) and is therefore not discussed further. The remaining experimental findings are discussed in more detail below.

3.2. Influence of NO_x and RH on SOA (Experiments: Tol-1 to Tol-4)

3.2.1. Influence of NO_x and RH on SOA Mass Formation

As shown in Figure 1a–d, the SOA mass generally declined non-linearly as $[NO_x]/[\Delta HC]$ increased in experiments Tol-1 to Tol-4; it was largely independent of $[NO_x]/[\Delta HC]$ under NP conditions ($[NO_x]/[\Delta HC] \leq 0.15$) but decreased with increasing $[NO_x]/[\Delta HC]$ under

NR conditions ($[\text{NO}_x]/[\Delta\text{HC}] > 0.15$). This suggests that the ongoing chemical reactions favoured the formation of more volatile organic products under NR conditions.

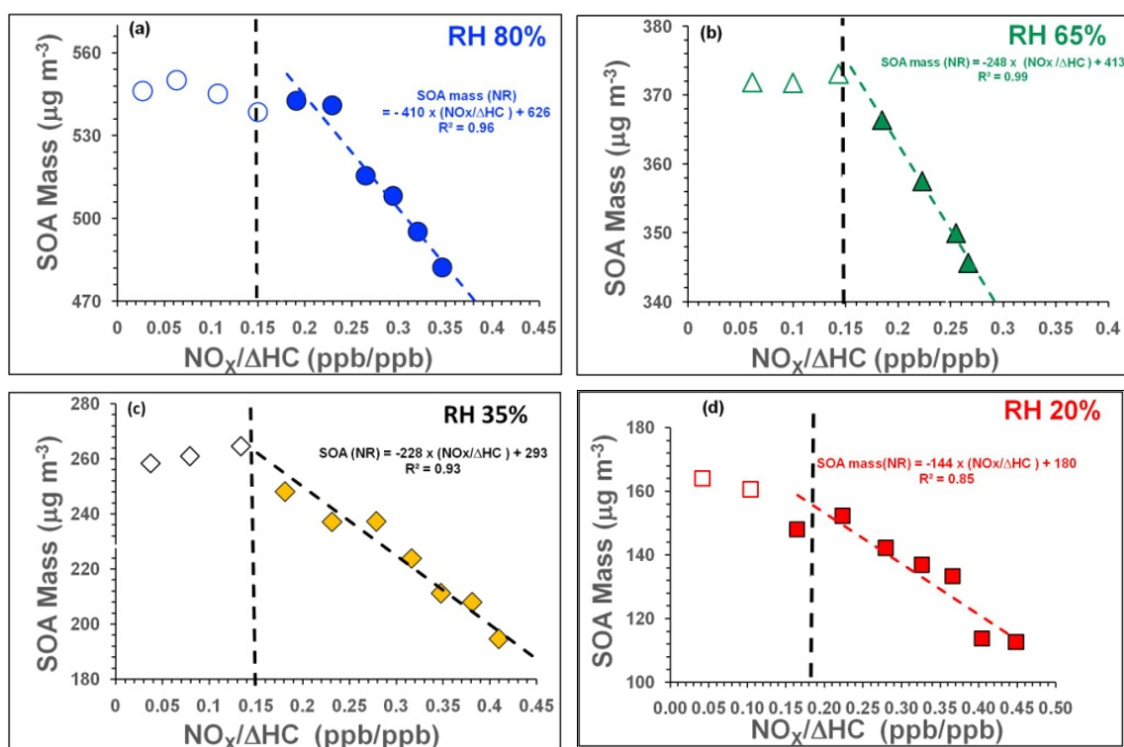


Figure 1. (a–d): SOA mass formed as a function of $[\text{NO}_x]/[\Delta\text{HC}]$ at (a) 80% RH, (b) 65% RH, (c) 35% RH, and (d) 20% RH. Empty and filled symbols show results for NP and NR SOA, respectively. Dashed lines are included to guide the eye.

Conversely, the light absorption of the SOA (measured in terms of the aerosol absorption coefficient at 405 nm, i.e., $B_{\text{abs},405}$) generally increased with $[\text{NO}_x]/[\Delta\text{HC}]$, irrespective of NP or NR regimes. However, the increase was again non-linear; in experiments Tol-1–Tol-4, B_{abs} increased moderately with increasing $[\text{NO}_x]/[\Delta\text{HC}]$ under NP conditions but the increase became steeper under NR conditions, as shown in Figure 2. These trends confirm the formation of some prominent SOA chromophores due to the influence of NO_x on toluene-OH chemistry in the presence of water.

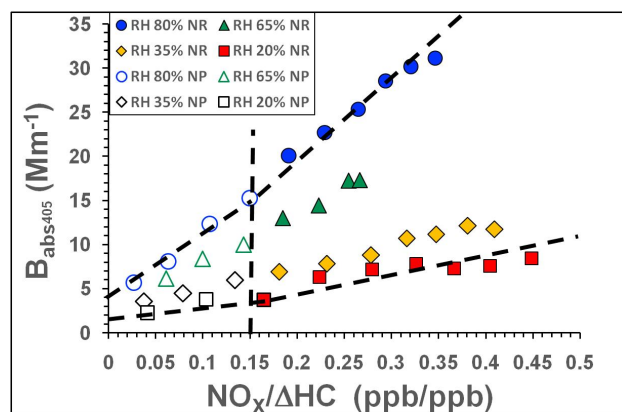


Figure 2. The aerosol absorption coefficient B_{abs} as a function of $[\text{NO}_x]/[\Delta\text{HC}]$ at 80% RH, 65% RH, 35% RH and 20% RH. Empty and filled symbols show results for NP and NR SOA, respectively. Dashed lines are included to guide the eye.

The results shown in Figures 1 and 2 indicate that $[\text{NO}_x]/[\Delta\text{HC}]$ has two opposing effects on SOA formation; higher $[\text{NO}_x]/[\Delta\text{HC}]$ levels promote the formation of light absorbing chromophores (browning molecules) but reduce that of molecules contributing to SOA mass.

The effect of RH on the SOA mass was also non-linear. Under both NP and NR conditions, the SOA mass increased with the RH (see Figure S2 in Supplementary Materials) but the SOA mass was always higher under NP conditions than NR conditions, all else being equal. The increase in the SOA mass with the RH can be attributed to several factors including the amount of toluene reacted, the initial OH concentration, and the hygroscopic growth of SOA. As the RH increases, so too does the OH concentration in the reaction zone of the GO:PAM flow-tube, leading to higher toluene consumption and thus greater SOA mass formation. Water-mediated OH chemistry may also have contributed to SOA mass formation at the highest tested RH (80%). The effect of NO_x on the SOA mass was comparatively small (the SOA masses at the highest and lowest NO_x concentrations differed by <20%) and may be linked to the formation of nitrogen-rich SOA via RO_2+NO reactions. These processes influenced the composition of the product compounds, for example by increasing the abundance of organo-nitrates (RONO_2) at high NO_x concentrations. They also influenced the distribution of common products such as carbonyls ($\text{R}=\text{O}$) [45]. Because the SOA mass depends on the distribution of product vapor pressures, it would be expected to be influenced by the $[\text{NO}_x]/[\Delta\text{HC}]$ ratio, especially in the NR regime.

3.2.2. Influence of NO_x and RH on Light Absorption

As outlined previously (see Section 3.2.1 and Figure 2), NO_x promoted the formation of BrC-rich SOA. However, unlike the SOA mass, B_{abs} increased steadily with $[\text{NO}_x]/[\Delta\text{HC}]$ in the NP regime at the higher RH. Both the absolute values of B_{abs} and the slope of the plot of B_{abs} against RH became higher as the NO_x increased from NP to NR regimes. The trend towards higher B_{abs} values at higher RH is consistent with the trends observed for mass (see Figure 1). These results indicate that NO_x - and water-mediated toluene-OH chemistry promote both SOA mass formation and BrC formation at high RH values (e.g., 80%) due to the synergistic effects of water vapour and high OH concentrations on water-mediated OH chemistry. These effects can also be seen in Figure 3, which shows the variation of B_{abs} with RH under NR and NP conditions. Under NP conditions, B_{abs} increases linearly with RH, but under NR conditions the increase becomes steeper and non-linear, as shown in Figure 3. These results suggest that the effect of RH on B_{abs} (and thus BrC formation) is primarily due to water-mediated OH chemistry, and that the effect of NO_x on the formation of BrC compounds (i.e., chromophores) is modest. In addition, the sudden non-linear increase in B_{abs} at high RH (80%) under the NR regimes suggests that water-mediated NO_x chemistry plays a significant role in the formation of strongly light-absorbing compounds under these conditions without greatly increasing the total SOA mass; the SOA masses under the NP and NR regimes were within 10–20% of each other at the same RH (see Figure S2 in Supplementary Materials).

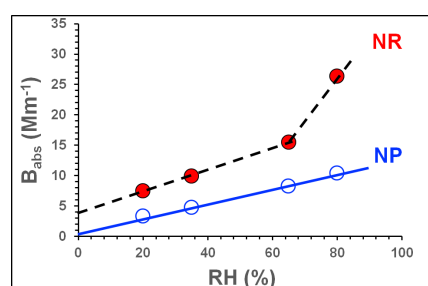


Figure 3. B_{abs} as a function of RH in the NP and NR SOA formation regimes. NP (empty) and NR (filled) symbols are blue and red coloured, respectively. The solid and dashed lines are included to guide the eye.

The mass absorption cross section (MAC) of the SOA was estimated by normalizing B_{abs} against the SOA mass (see Table S2 in the Supplementary Materials and Table 3). Figure 4 clearly shows that like the B_{abs} , MAC of the SOA increased with $[NO_x]/[\Delta HC]$ under all RH conditions, with a clear “switching point” at $[NO_x]/[\Delta HC] = 0.15$. The clear increase in MAC with $[NO_x]/[\Delta HC]$ in the NP regime shows that NO_x played a significant role in chromophore formation chemistry even when its concentration was low and that more strongly light-absorbing chromophores were formed as $[NO_x]/[\Delta HC]$ increased. In other words, the light absorption potential of the formed SOA was highly sensitive to the $[NO_x]/[\Delta HC]$ ratio under both NP and NR regimes. Interestingly, the increase in MAC due to the influence of NO_x under NP conditions was independent of RH. At 80% RH, the increase in MAC with increasing $[NO_x]/[\Delta HC]$ was slightly steeper under NR conditions than under NP conditions. However, the difference between NP and NR conditions was less clear at lower RH values (e.g., 35% RH).

Table 3. SOA Properties under various experimental conditions in the NP and NR regimes.

Exp. ID	RH (%)	Avg. SOA Mass ($\mu\text{g m}^{-3}$)		Avg. $NO_x/\Delta HC$		Avg. ALW* ($\mu\text{g m}^{-3}$)		Avg. SOA Mass# (dry) ($\mu\text{g m}^{-3}$)		Avg. B_{abs405} (Mm^{-1})		Dry SOA MAC_{405} ($m^2 g^{-1}$)		ALW+SOA MAC_{405} ($m^2 g^{-1}$)	
		NP	NR	NP	NR	NP	NR	NP	NR	NP	NR	NP	NR	NP	NR
Tol-1	80	545	508	0.094	0.288	167	155	378	353	10.3	28.0	0.027	0.079	0.019	0.055
Tol-2	65	372	342	0.094	0.288	84	77	289	265	8.2	19.0	0.028	0.072	0.022	0.056
Tol-3	35	261	227	0.094	0.288	19	17	242	210	4.7	10.0	0.019	0.048	0.018	0.044
Tol-4	20	158	139	0.094	0.288	6	3	152	136	3.3	6.5	0.022	0.048	0.021	0.047

ALW* = Aerosol Liquid Water calculated by Extended AIM Aerosol Thermodynamics Model [44]. Avg. SOA Mass# (dry) = ((SOA Mass at SMPS)—ALW).

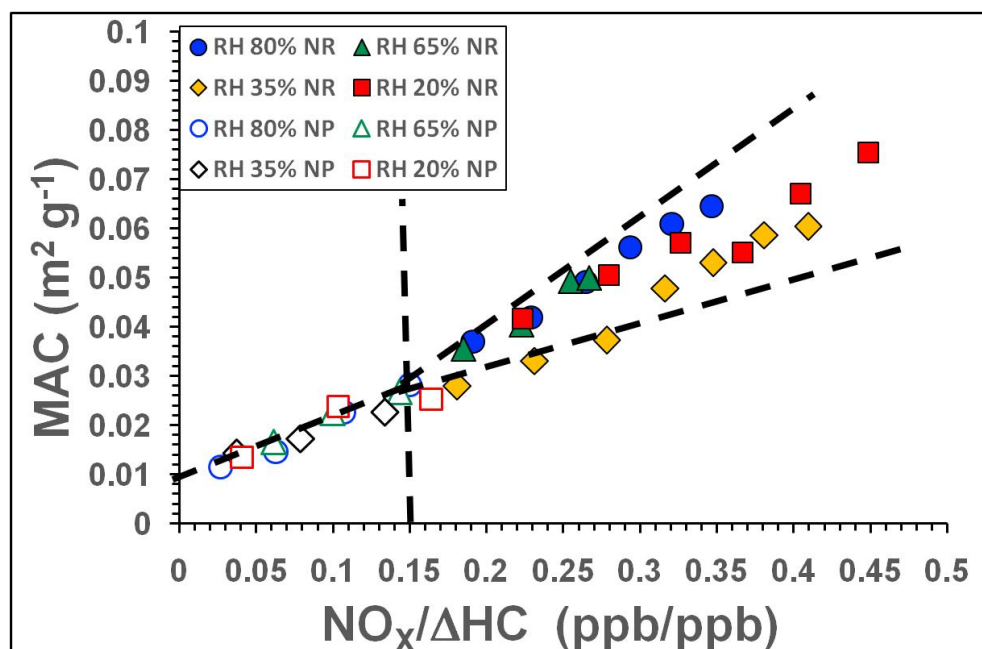


Figure 4. MAC (mass absorption cross-section) as a function of the $[NO_x]/[\Delta HC]$ ratio at 80%, 65%, 35% and 20% RH. Empty and filled symbols show results for NP and NR SOA, respectively. The dashed lines are included to guide the eye.

Figure 5 shows how the influence of RH on the MAC clearly differed between the NP and NR regimes. This outcome is not easily explained and suggests the influence of two

or more competing processes, notably (i) hygroscopic growth of the formed SOA, which increases the SOA mass through the incorporation of aerosol liquid water (ALW); and (ii) the water-mediated chemistry of the toluene-NO_x-OH system and its effects on the composition and hygroscopicity of the formed SOA.

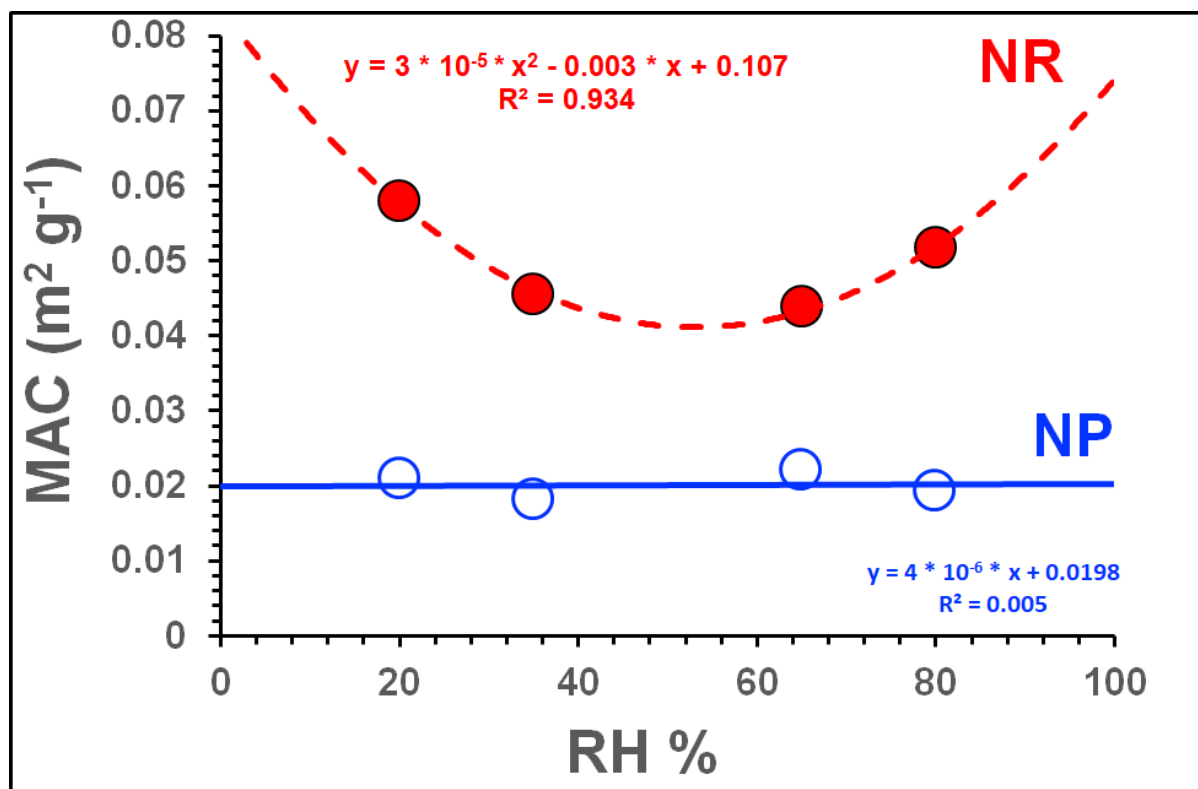


Figure 5. MAC as a function of RH in the NP and NR SOA formation regimes. Results for the NP and NR regimes are plotted using empty blue and filled red circles, respectively. Solid and dashed lines are included to guide the eye.

At a given RH, the B_{abs} value of the SOA reflects only the number of chromophores formed as a result of toluene-NO_x-OH-water-mediated chemistry. The increase in B_{abs} with $[\text{NO}_x]/[\Delta\text{HC}]$ indicates that NO_x-water chemistry has an important effect on MAC at high RH levels. At the same time, hygroscopic growth at high RH enhances the contribution of ALW to the SOA mass measured by the SMPS, which is calculated using the SOA density functions of Ng et al. [20]. This in turn leads to underestimation of the MAC at high RH. These two processes may have opposing effects on the MAC because hygroscopic growth increases SOA mass, while toluene-NO_x-OH-water-mediated chemistry promotes BrC formation. At high RH, hygroscopic growth reduces MAC, while VOC-NO_x-OH-H₂O-mediated chemistry increases B_{abs} .

The trends in SOA formation observed in experiments Tol-1 to Tol-4 at RH values of 80% to 20% under NP and NR regimes were similar to those reported by Liu P. et al. [33]. However, the mass enhancement factor (MEF) determined at the lowest RH examined in our experiments (20%; see Figure S3 of the Supplementary Materials) was significantly higher than that reported by Liu P. et al. [33], which is notable because these authors studied a very hygroscopic toluene SOA formed at almost 1% RH and examined its absorption of water at higher RH values. Therefore, hygroscopic growth alone cannot explain the high MEF observed in this work. Instead, the MEF trends observed here can be attributed to several factors that were discussed above, namely: (i) the increase in the SOA mass due to increased concentrations of both OH radicals and reacted toluene $[\Delta\text{HC}]$ at higher RH values; (ii) the greater hygroscopicity of SOA formed at higher RH values and more

extensive heterogeneous oxidation of SOA due to aging; and (iii) the influence of NO_x chemistry on the gas-aerosol partitioning and hygroscopicity of the SOA. In addition, Liu T. et al. [34] showed that increasing OH exposure during SOA formation caused a sharp increase in ALW at constant RH in the low NO_x regime. However, when normalized against the dry SOA mass, the ALW did not increase significantly as the OH concentration increased, indicating that the hygroscopicity of toluene SOA (i.e., its capacity to absorb water) at a given RH was independent of the OH concentration and was thus unaffected by OH-water mediated chemistry. This in turn implies that the large differences between the MEF values obtained in this work and those reported by Liu P. et al. [33] can be attributed to the water-mediated toluene-OH chemistry of NP SOA. Additionally, since the NP and NR MEF curves almost overlapped each other, it can be assumed that the hygroscopicity of NR SOA was similarly insensitive to high OH exposure at high RH levels, and also to high NO_x concentrations. We therefore used the parametrization of Liu P. et al. [33] (See Equation (S18) in the Supplementary Materials of Liu P. et al.) to estimate the ALW contents of the SOAs prepared in this work, which are listed in Table 3.

3.2.3. Influence of NO_x and RH on Light Scattering

The SOA light scattering coefficient (B_{scat}) decreased non-linearly in response to linear increases in the NO_x concentration at a constant RH. This decrease correlated non-linearly with the $[\text{NO}_x]/[\Delta\text{HC}]$ ratio at RH values between 80% and 20%, as shown in Figure 6. Interestingly, the non-linearity in these curves again occurred at an $[\text{NO}_x]/[\Delta\text{HC}]$ value of around 0.15. The total scattering (B_{scat}) of NP SOA did not vary greatly with $[\text{NO}_x]/[\Delta\text{HC}]$ at constant RH. However, the B_{scat} for NR SOA decreased with increasing $[\text{NO}_x]/[\Delta\text{HC}]$. This decreasing trend in B_{scat} values mirrored that seen for the SOA mass (see Figure 1a–d) and can be attributed to the reduction in the mass (see the slopes of the parameterization of NR SOA against $[\text{NO}_x]/[\Delta\text{HC}]$ in Table S2 of the Supplementary Materials) and surface area (data not shown) of the SOA at higher RH values.

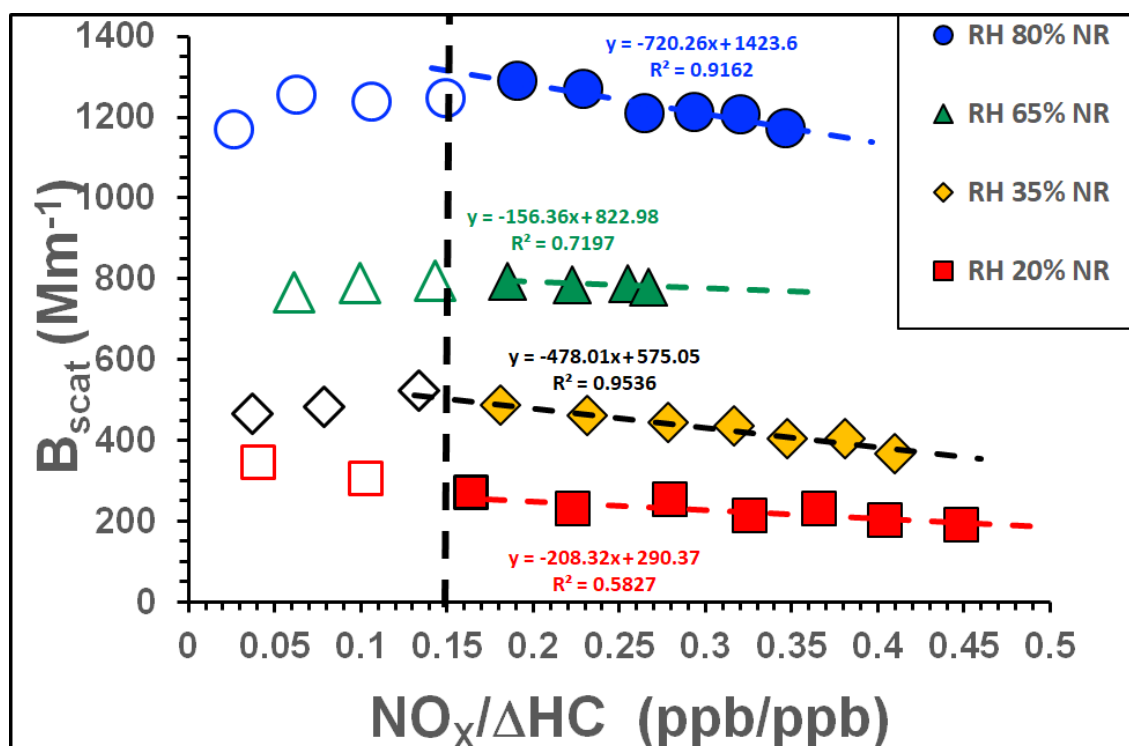


Figure 6. B_{scat} as a function of the NO_x to reacted toluene ratio ($[\text{NO}_x]/[\Delta\text{HC}]$) at 80% RH, 65% RH, 35% RH and 20% RH. Empty and filled symbols show results for NP and NR SOA, respectively. The dashed lines are included to guide the eye.

In both the NP and NR regimes, B_{scat} increased non-linearly with RH (see Figure S4 of the Supplementary Materials), with the non-linearity becoming apparent above 65% RH; the B_{scat} at 80% RH was substantially higher than at lower RH values. This can be attributed to the high ALW content of the SOA at 80% RH (see Figure S5 in Supplementary Materials). As discussed previously, because the SOA hygroscopicity was similar in the NP and NR regimes, the ALW showed similar responses to increasing RH in both cases (see Figure S5).

As shown in Figure 7, the MSC (mass scattering cross-section) of the SOA varied non-linearly with increasing $[\text{NO}_x]/[\Delta\text{HC}]$ and RH. In the NP regime, MSC increased slightly with increasing $[\text{NO}_x]/[\Delta\text{HC}]$ for all RH values bar the lowest (20% RH), in which case the MSC decreased slightly as $[\text{NO}_x]/[\Delta\text{HC}]$ increased. In the NR regime, MSC increased moderately with $[\text{NO}_x]/[\Delta\text{HC}]$ at 80% and 65% RH but decreased as $[\text{NO}_x]/[\Delta\text{HC}]$ increased at 20% RH and did not vary appreciably with increasing $[\text{NO}_x]/[\Delta\text{HC}]$ at 35% RH. These results clearly reveal a switching point in the relationship between MSC and $[\text{NO}_x]/[\Delta\text{HC}]$ at around 35% RH.

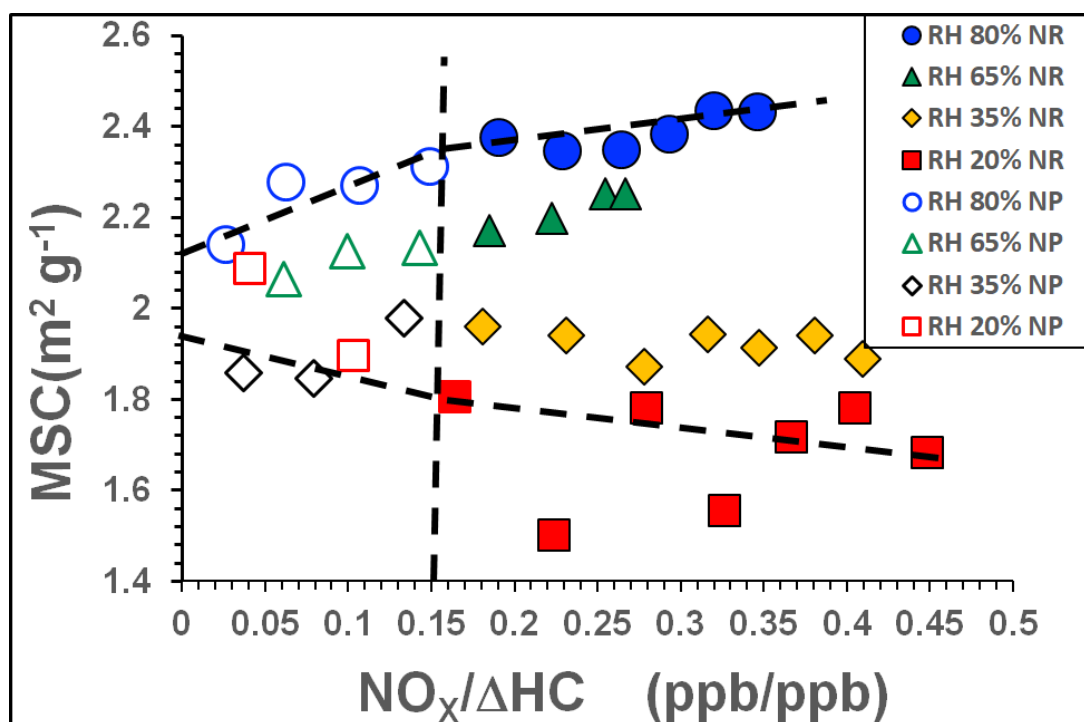


Figure 7. MSC as a function of the NO_x to reacted toluene ratio ($[\text{NO}_x]/[\Delta\text{HC}]$) at 80% RH, 65% RH, 35% RH and 20% RH. Empty and filled symbols show results for NP and NR SOA, respectively. The solid and dashed lines are included to guide the eye.

Plotting the MSC as a function of the RH (see Figure S6 of the Supplementary Materials) revealed a positive linear relationship between these two quantities in both the NP and NR regimes, so the scattering potential of the SOA was greatest at high RH. This can be attributed to the greater adsorption of water onto the SOA at higher RH values. Interestingly, however, the slope of the plot was steeper in the NR case (see Figure S6 in Supplementary Materials). As a result, the NR MSC was lower than the NP MSC when the RH was 35% or less, but the opposite was true at higher RH values. The light scattering potential of the NR SOA was thus more sensitive to the RH than that of the NP SOA. This outcome can be attributed to the ALW content of the SOA, which is higher in the NR case at high RH (>35%) and in the NP case at low RH (35% or less). In other words, the NR SOA absorbed more water and became more strongly scattering at high RH, while the reverse

was true at low RH. This may indicate that the molecular composition of the SOA (i.e., its product distribution) changes significantly between 65% RH and 35% RH.

As expected, the single scattering albedo (SSA) of both NP and NR SOA was significantly affected by both NO_x and water vapour. Generally, the SSA values decreased as $[\text{NO}_x]/[\Delta\text{HC}]$ increased for both NP and NR SOA (see Figure S7 in Supplementary Materials) at constant RH. However, in the NR case there was a clear change in the SSA trend at an $[\text{NO}_x]/[\Delta\text{HC}]$ ratio of 0.15. Like the MAC, the SSA was insensitive to RH in the NP case but not in the NR case, for which the SSA was lowest at 20% RH (see Figure S8 in the Supplementary Materials). This indicates that the relative contribution of absorption to the total light extinction by SOA was enhanced under drier conditions in the NR regime. These results suggest that water mediated toluene- NO_x -OH chemistry increases the scattering potential of toluene SOA in the NR regime by substantially changing its composition, presumably by promoting the formation of more or stronger chromophores.

3.3. Influence of NH_3 and NO_x on SOA at High RH (Experiments: Tol-5 and Tol-6)

3.3.1. Influence of NH_3 and NO_x on SOA Mass at 80% RH

In experiments Tol-5 and Tol-6 (see Tables 1 and 2), the RH was fixed at 80% and the NO_x concentration was fixed at 61 ppb and 360 ppb, respectively, corresponding to $[\text{NO}_x]/[\Delta\text{HC}]$ ratios of 0.05 (NP SOA regime) and 0.31 (NR SOA regime). The input NH_3 concentration was ramped from 42 ppb, corresponding to an $[\text{NH}_3]/[\Delta\text{HC}]$ ratio of 0.04, to 203 ppb, corresponding to an $[\text{NH}_3]/[\Delta\text{HC}]$ ratio of 0.18 at 80% RH. The secondary brown carbon (SBrC) formation in these experiments showed unique trends that were not previously observed. First, for low NO_x scenario (NP), the SOA mass against $[\text{NH}_3]/[\Delta\text{HC}]$ ratio increase showed a large peak at $[\text{NH}_3]/[\Delta\text{HC}] \sim 0.13$ as shown in Figure 8. It is likely due to the formation of ammonium nitrate in toluene- NH_3 -OH system at low NO_x reported by Qi X. et al. [47], where addition of NH_3 enhanced the number concentration, average SOA diameter, and extinction and scattering coefficients due to the formation of significant amounts of condensable ammonium nitrate and nitrogen-containing (NOC) compounds.

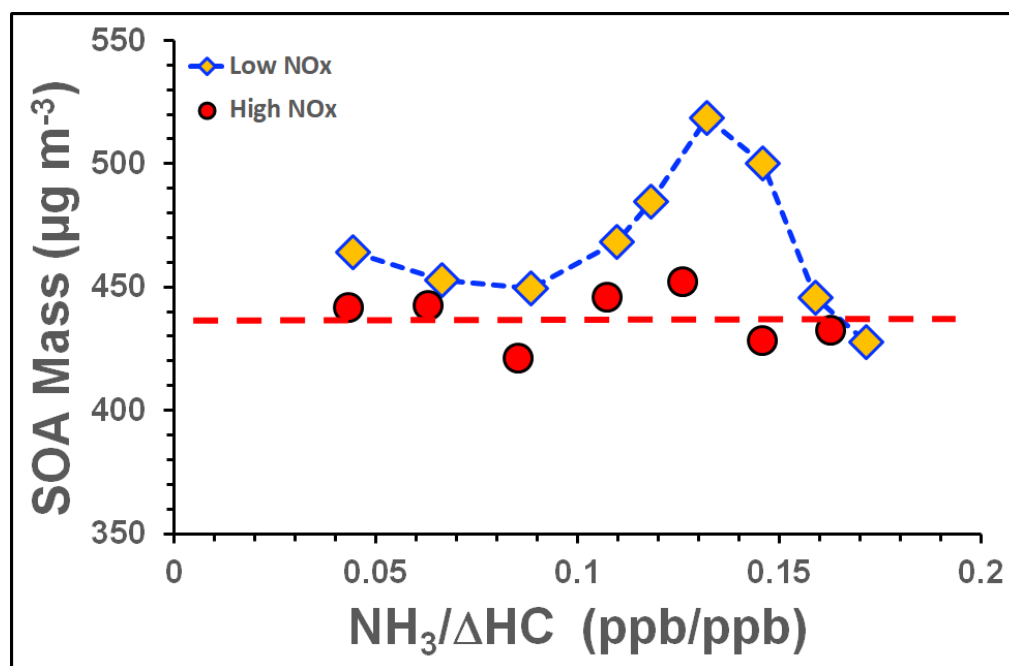


Figure 8. SOA mass as a function of the ($[\text{NH}_3]/[\Delta\text{HC}]$) ratio at 80% RH under low and high NO_x scenarios. Blue and red dotted lines are the eye guiding lines for low and high NO_x scenarios, respectively.

On the other hand, SOA mass was relatively lower for a high NO_x scenario than in a low NO_x scenario and varied insignificantly (apparently constant $\sim 435 \mu\text{g m}^{-3}$) when

$[\text{NH}_3]/[\Delta\text{HC}]$ increased as shown in Figure 8. This is consistent with the SOA mass formed in NP and NR regimes in experiments Tol-1 to Tol-4. These suggest that overall NH_3 had little influence on SOA mass at high NO_x scenario (e.g., NR regime).

3.3.2. Influence of NH_3 , NO_x on SOA Light Absorption at 80% RH

Two results shown in Figures 9 and 10 are particularly noteworthy: (i) the B_{abs} and MAC in the low NO_x (Tol-5) also showed similar behaviour as SOA mass (see Figure 8) in response to increasing $[\text{NH}_3]/[\Delta\text{HC}]$ but peaked at $[\text{NH}_3]/[\Delta\text{HC}] \sim 0.11$, however, (ii) the B_{abs} and MAC in high NO_x (Tol-6) were much higher than low NO_x experiment (Tol-5) and SOA mass in the high NO_x case (see Figure 8). The similar behaviors of B_{abs} and MAC as functions of $[\text{NH}_3]/[\Delta\text{HC}]$ suggest that N-H-containing organic chromophores (e.g., cyclic amines such as azo compounds) with similar light absorption profiles were formed in the low NO_x regime [48,49]. In the high NO_x regime, SOA formation via the NO_x -water mediated chemistry appears to dominate because the B_{abs} and MAC in this case behaved similarly to those of the NR SOA formed in experiments Tol-1 to Tol-4. That is to say, B_{abs} and MAC were independent of $[\text{NH}_3]/[\Delta\text{HC}]$ in the high NO_x regime and almost constant ($B_{\text{abs}} \sim 40 \text{ Mm}^{-1}$, $\text{MAC} \sim 0.09 \text{ m}^2 \text{ g}^{-1}$).

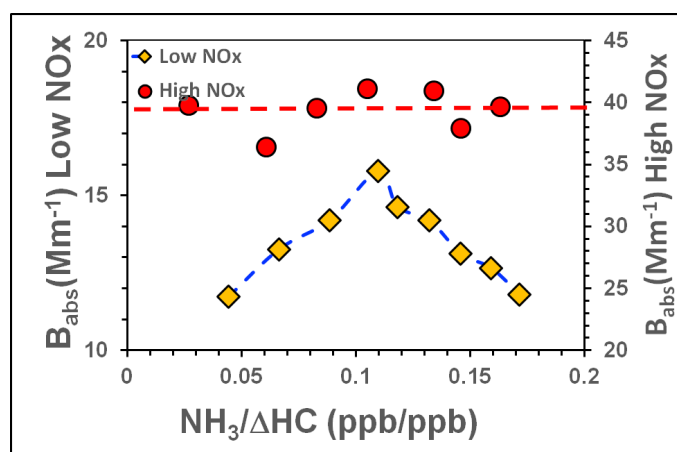


Figure 9. B_{abs} as a function of the ($[\text{NH}_3]/[\Delta\text{HC}]$) ratio at 80% RH under low and high NO_x scenarios. Blue and red dotted lines are the eye guiding lines for low and high NO_x scenarios, respectively. The dashed lines are included to guide the eye.

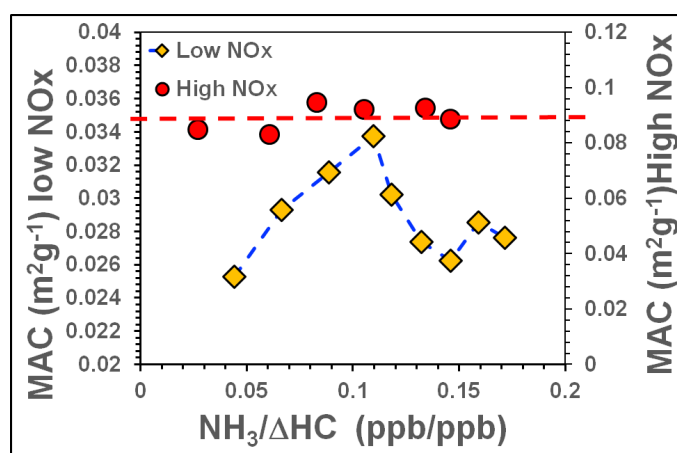


Figure 10. MAC as a function of the ($[\text{NH}_3]/[\Delta\text{HC}]$) ratio at 80% RH under low and high NO_x scenarios. Blue and red dotted lines are the eye guiding lines for low and high NO_x scenarios, respectively. The dashed lines are included to guide the eye.

3.3.3. Influence of NH_3 and NO_x on SOA Light Scattering at 80% RH

Interestingly, the scattering coefficient (B_{scat}) and potential (MSC) were both high and did not respond to increases in $[\text{NH}_3]/[\Delta\text{HC}]$ in the same way as B_{abs} and the SOA mass under either high or low NO_x regimes (see Figure S9a,b in the Supplementary Materials). B_{scat} and MSC initially increased with $[\text{NH}_3]/[\Delta\text{HC}]$ in both high and low NO_x regimes but then remained almost constant when the $[\text{NH}_3]/[\Delta\text{HC}]$ ratio rose above 0.11. In other words, although the SOA mass decreased as the $[\text{NH}_3]/[\Delta\text{HC}]$ ratio increased above 0.13, B_{scat} and MSC did not change significantly. These outcomes can potentially be attributed to the presence of highly scattering coatings of condensed ammonium nitrate on SOA in both NO_x regimes. The MSC for SOA formed under the low NO_x regime was significantly higher than in the high NO_x regime. However, it is noteworthy that in both regimes the MSC was significantly higher than in any previous experiment that is Tol-1 to Tol-4. B_{scat} was also lower in the high NO_x regime. This is probably because the effects of high NO_x concentrations, which favour the formation of comparatively volatile organo-nitrates, outweigh those of organo-amines from NH_3 reaction during SOA formation. These findings show that NH_4NO_3 strongly affects the formation and properties of SOA under the NP regime, and that the presence of NH_3 under high NO_x conditions promotes the formation of more light-absorbing SOA. Previous studies have similarly concluded that NH_3 increases the O:C and N:C ratios of compounds formed by toluene-OH water-mediated chemistry and promotes the formation of SOA compounds containing carbonyl and carboxylic acid functional groups under low NO_x conditions [48,49].

Figure 11 summarizes the complex influences of NH_3 on the light absorption and scattering characteristics (i.e., MAC, MSC, B_{abs} , and B_{scat}) of toluene SOA under the NP and NR regimes. First, NH_3 clearly promotes SOA browning because both B_{abs} and MAC increase with the NH_3 concentration under both NP and NR conditions. Second, the scattering of toluene SOA was thought to be synergistically promoted by NH_3 via NH_4NO_3 formation under the NP regime (i.e., in low NO_x scenarios), which is consistent with Qi X. et al. [47]. Conversely, NH_3 did not influence the scattering properties of toluene SOA under the NR regime.

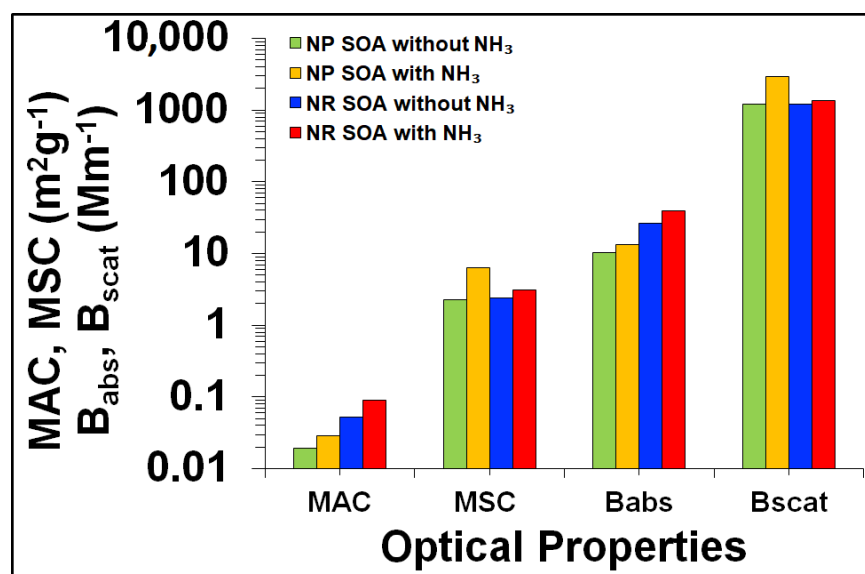


Figure 11. Summary of the effects of NH_3 on the optical characteristics of toluene SOA, i.e., MAC, MSC, B_{abs} and B_{scat} at 80% RH under low and high NO_x conditions (data are plotted using a log scale).

Finally, the presence of NH_3 led to higher B_{scat} and lower B_{abs} values under low NO_x conditions, with the reverse being true under high NO_x conditions. These results indicate that NH_3 increases the O:C content of the SOA under low NO_x conditions and the N:C ratio of the SOA under high NO_x conditions.

3.4. Influence of NO_x Acidity and RH on SOA (Experiments: Tol-7 to Tol-9)

3.4.1. Influence of NO_x Acidity and RH on SOA Mass

As shown in Figure 12a–c, SOA formation in the H_2SO_4 -seeded experiments with NO_x ramps (see Tables 1 and 2; experiments Tol-7 to Tol-9) clearly depended on both NO_x and RH. As in the case without H_2SO_4 seeding (experiments Tol-1 to Tol-4; see Figure 1a–d), the dependence of the SOA mass on $[\text{NO}_x]/[\Delta\text{HC}]$ differed markedly between NP and NR conditions. However, the response of the SOA mass to increases in the $[\text{NO}_x]/[\Delta\text{HC}]$ ratio also differed in some respects from that seen under non-seeded conditions (see Figure 1a–d). The similarities are due to the fact that SOA is formed by toluene- NO_x chemistry in both cases, while the differences can be attributed to the impact of acidity-mediated heterogeneous chemistry and NO_x on SOA formation [50–52]. In the acid-seeded experiment with 80% RH (Tol-7), the SOA mass increased with the $[\text{NO}_x]/[\Delta\text{HC}]$ ratio under NP conditions but then became independent of $[\text{NO}_x]/[\Delta\text{HC}]$ under NR conditions (see Figure 12a). Conversely, in the H_2SO_4 seeded experiments at 65% and 20% RH (Tol-8 and Tol-9), the SOA mass decreased significantly as $[\text{NO}_x]/[\Delta\text{HC}]$ increased under NR conditions but did not vary greatly with $[\text{NO}_x]/[\Delta\text{HC}]$ under NP conditions. Under both NP and NR conditions with acid seeding, the SOA mass at 80% RH was lower than in the corresponding non-seeded experiments whereas the opposite was true at 20% RH (see Figure S10a,b in the Supplementary Materials). At 65% RH, the SOA masses in the H_2SO_4 -seeded and non-seeded experiments were comparable. To better understand these outcomes, the influence of ALW and pH on SOA mass formation was investigated (see Figure S10c–f and Table S3 in the Supplementary Materials). This suggested that ALW (see Figure S10c,d) increased the availability of free acid, i.e., $[\text{H}^+]_{\text{free}}$ (see Figure S10e) formed by H_2SO_4 dissociation at all RH levels (see Table S3 in Supplementary Materials). Therefore, the pH of the SOA was lowest at the lowest RH (20%) (see Figure S10f in Supplementary Materials). Moreover, whereas both ALW and the SOA mass increased with RH, the acidity of the SOA decreased (i.e., its pH increased; see Figure S10a–e in Supplementary Materials). Accordingly, the SOA mass increase due to acidity was most pronounced (30% in the NR case and 21% in the NP case) at the lowest pH at 20% RH. However, at 65% RH, the pH and SOA mass were both higher and acidity had no appreciable effect on the SOA mass, while at the highest pH (80% RH), acidity reduced the SOA mass significantly when compared to the non-seeded experiments—by 35% and 21% under NP and NR conditions, respectively. These results show that the effects of acidity on the formation and properties of SOA are complex. The observation that acid seeding and high RH (80%) caused NO_x to increase SOA formation in the NR regime but not in the NP regime (in the Tol-7 experiment) is unprecedented and contrary to the observed SOA formation behaviour in the absence of H_2SO_4 seeding (i.e., in the Tol-1 experiment). Deng et al. [51] reported that SOA mass was increased by acidic seeding when SOA loadings were low, but that this increase was not observed at higher SOA loadings. Additionally, Cao and Jang [52] reported that the mass of toluene SOA formed under low and intermediate NO_x conditions (which both fall within the NP regime as defined in this work) with acidic sulphate seeding was considerably higher (by ~15–21%) at low RH when compared to the case with neutral seeding, but was reduced at high RH (by ~38–48%). No significant particle acidity effect was observed in the high NO_x experiments in their study [52]. These results provide important new insights into the effects of NO_x , RH, and acidity on SOA formation and will thus facilitate better modelling of toluene SOA formation.

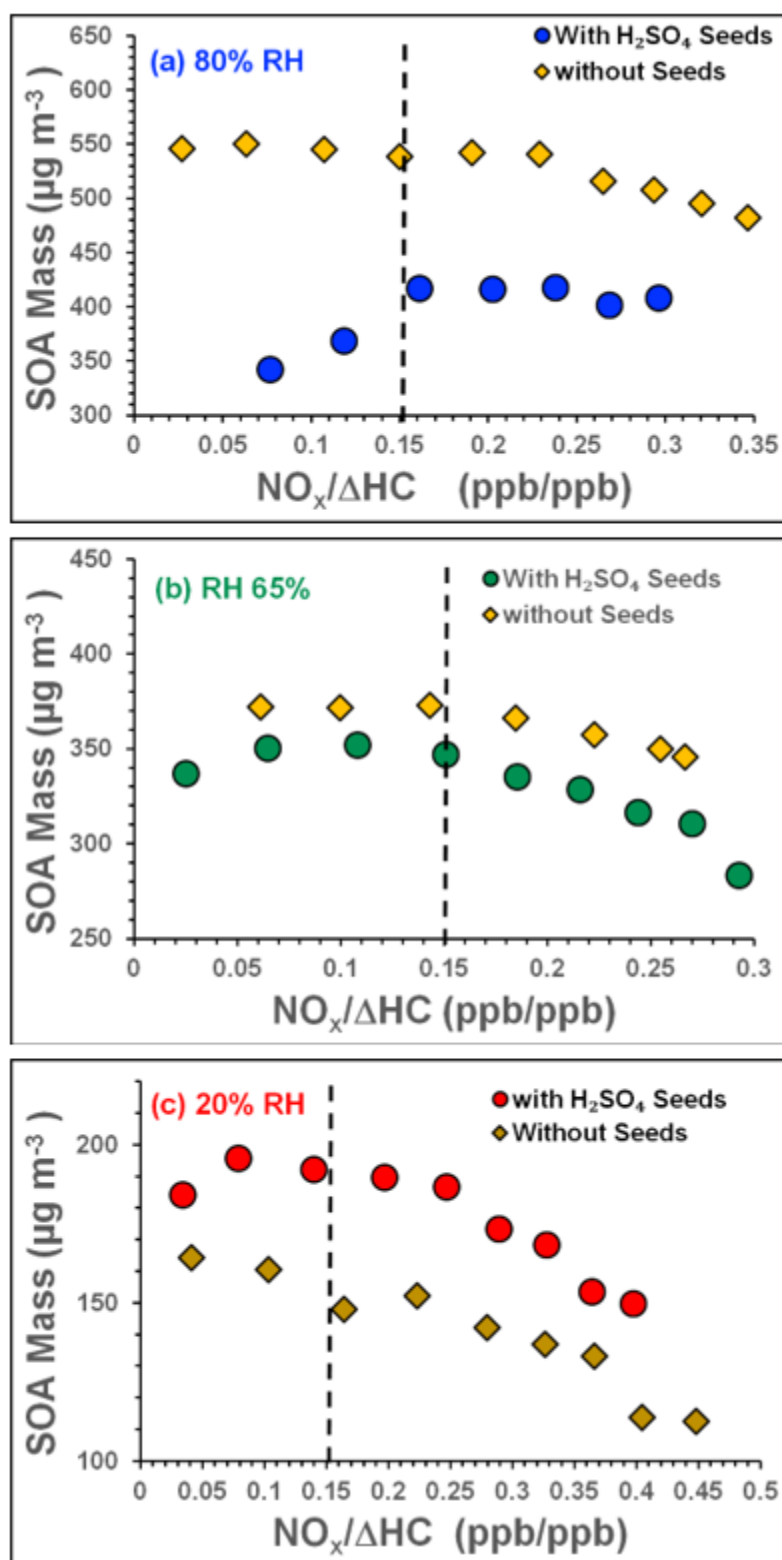


Figure 12. (a–c): SOA mass as a function of $\text{NO}_x/[\Delta\text{HC}]$ and the influence of acidity on SOA mass at (a) 80% RH, (b) 65% RH, and (c) 20% RH. The dashed lines are included to guide the eye.

3.4.2. Influence of NO_x Acidity and RH on SOA Light Absorption

We also investigated the influence of SOA mass, acidity, NO_x , and RH on the optical properties of toluene SOA. Figure 13a–f shows the B_{abs} and MAC of toluene SOA as functions of the $[\text{NO}_x]/[\Delta\text{HC}]$ ratio at three different RH values in the H_2SO_4 seeded

experiments (Tol-7, Tol-8, and Tol-9). As in the non-seeded experiments, B_{abs} increased with $[\text{NO}_x]/[\Delta\text{HC}]$ in the H_2SO_4 seeded experiments. However, the slope was slightly steeper in the seeded case and the absolute values of B_{abs} were approximately 2 Mm^{-1} higher at all RH values below 80% (See Figure 13a–c).

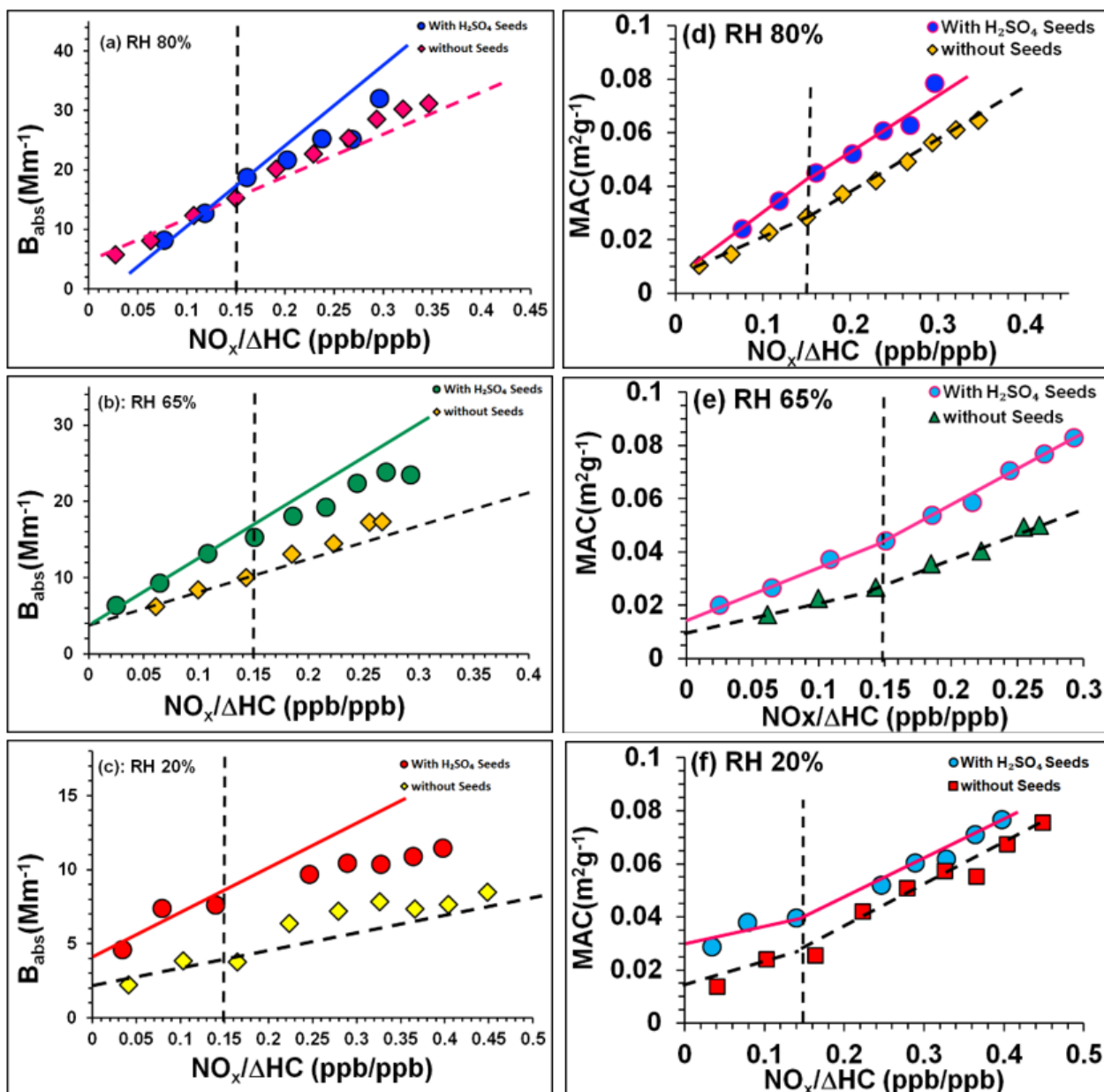


Figure 13. (a–f): Effects of acidity, NO_x and RH on the B_{abs} and MAC of toluene SOA. (i) B_{abs} as a function of $[\text{NO}_x]/[\Delta\text{HC}]$ in H_2SO_4 seeded and non-seeded experiments at (a) 80%, (b) 65%, and (c) 20% RH. (ii) MAC as a function of $[\text{NO}_x]/[\Delta\text{HC}]$ in H_2SO_4 seeded and non-seeded experiments at (d) 80%, (e) 65%, and (f) 20% RH. The solid and dotted lines in Figure 13 (a–c) are eye guides showing the trends in B_{abs} for NP SOA in the H_2SO_4 seeded and non-seeded cases, respectively; eye guides for the NR case are not shown. Conversely, in Figure 13 (d–f), the solid and dotted lines are eye guides for both the NP and NR SOA in H_2SO_4 seeded and non-seeded experiments, respectively. The solid and dashed lines are included to guide the eye.

At 80% RH, the B_{abs} trends in the non-seeded (Tol-1) and H_2SO_4 seeded (Tol-7) experiments were almost identical, indicating that acidity had no obvious effect on B_{abs} under either the NP or the NR regime in this case. However, because SOA mass formation was

reduced under acidic conditions at 80% RH (see Figure 12a) and the MAC is the quotient of $[B_{\text{abs}}]$ and the SOA mass, the MAC was higher in the seeded case than in the non-seeded case (see Figure 13d). The MAC of acid-seeded SOA in the 65% and 20% RH cases (experiments Tol-8 and Tol-9, respectively) was also higher than in the corresponding non-seeded cases, as shown in Figure 13e,f. This indicates that acidity plays an important role in SOA browning. The effect of RH on the light absorbing properties of toluene SOA formed with acid seeding is clearly shown in Figure 14a–c: under NP conditions, the MAC at all three RH values was almost identical to that in the corresponding non-seeded experiments, but the MAC in the H_2SO_4 -seeded experiments was generally higher than that in the corresponding non-seeded experiments and increased as the RH decreased. The high MAC of acidic SOA at lower RH values is tentatively linked to the formation of organo-sulphate chromophores, which is suggested to be governed by two major parameters: (i) the pH of the SOA aqueous phase, and (ii) the ratio of $[\text{H}^+]_{\text{free}}$ (the concentration of free protons in the aqueous phase) to the SOA mass. Under NP conditions, the highest acidity (i.e., the lowest pH) and the highest $[\text{H}^+]_{\text{free}} / \text{SOA mass}$ ratio were both observed with seeding, as shown in Figures 13e and 14c, supporting our hypothesis. In addition, a modelling study conducted by McNeill et al. [53] suggested that organo-sulphate formation was maximized at low pH and low RH (<60%), i.e., when the aerosol was more concentrated. Conversely, under NR conditions the MAC of non-seeded SOA reached a minimum at an intermediate RH (65%), whereas the MAC of the H_2SO_4 seeded SOA peaked at the same RH (65%) and was lowest at 80% RH (see Figure 14b). These contrasting trends for seeded and non-seeded SOA under NR conditions are interesting and suggest that NO_x has a strong influence on light absorption at the intermediate RH (65%). These observations indicate that the browning of toluene SOA is driven by complex interactions between the effects of acidity, NO_x , and water vapor.

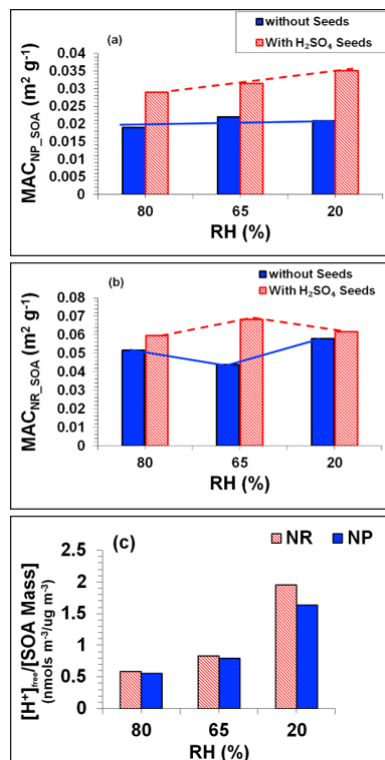


Figure 14. (a–c): Effects of water vapour and acidity on the MAC of toluene SOA. (a) MAC of NP SOA for the H_2SO_4 seeded and non-seeded experiments at the three RHs; (b) MAC of NR SOA for the H_2SO_4 seeded and non-seeded experiments at the three RHs; (c) concentration of $[\text{H}^+]$ (free acid) per unit SOA mass available in aqueous for heterogeneous chemistry at the three RHs. The solid and dashed lines are eye guides.

3.4.3. Influence of NO_x Acidity and RH on SOA Light Scattering

The light scattering characteristics of toluene SOA were also significantly influenced by H₂SO₄ seeding under various NO_x and RH conditions. The increase in B_{scat} with [NO_x]/[ΔHC] mirrored that of the SOA mass in all three H₂SO₄ seeded experiments (e.g., Tol-7, Tol-8 and Tol-9) (see Figure S11 in the Supplementary Materials). Upon comparing the seeded experiments to their non-seeded counterparts (Tol-1, Tol-2 and Tol-4, respectively), it can be seen that the response of B_{scat} to increasing [NO_x]/[ΔHC] differs and that acid seeding increased the absolute value of B_{scat} by factors of 1.25–2.5 in the NP regime and 1.5 to 3 in the NR regime (see Figure 15a,b). These increases in B_{scat} can be attributed to the presence of sulfuric acid seeds, which are likely to have increased the surface area and scattering potential of the formed SOA. The relative enhancement of B_{scat} in the H₂SO₄-seeded SOA was highest (2.5- to 3-fold) at the lowest RH (20%) indicating that the contribution of H₂SO₄ seeds to the aerosol mass fraction was highest at 20% RH. The response of the MSC to increases in [NO_x]/[ΔHC] was similar in both the H₂SO₄ seeded and non-seeded experiments (see Figure S12a,b in the Supplementary Materials). However, like the B_{scat} values, the absolute MSC values were significantly higher in the H₂SO₄ seeded experiments than in their non-seeded counterparts, under both NP and NR conditions (see Figure S12 in the Supplementary Materials). A rationale for the higher MSC in the seeded case is that H₂SO₄ also acts as a strongly scattering substance and increases the surface area of the resulting SOA. The highest MSC values were observed at the intermediate RH (65%) in both the NP and NR SOA regimes (see Figure S12a,b). However, the effects of acidity and RH on the chemical composition of the SOA and the resulting changes in its light scattering properties remain unclear. It seems most likely that the higher values of B_{scat} and MSC observed for seeded SOA under both NP and NR conditions can be mainly attributed to the enhancement of surface growth of SOA particles caused by H₂SO₄ seeds.

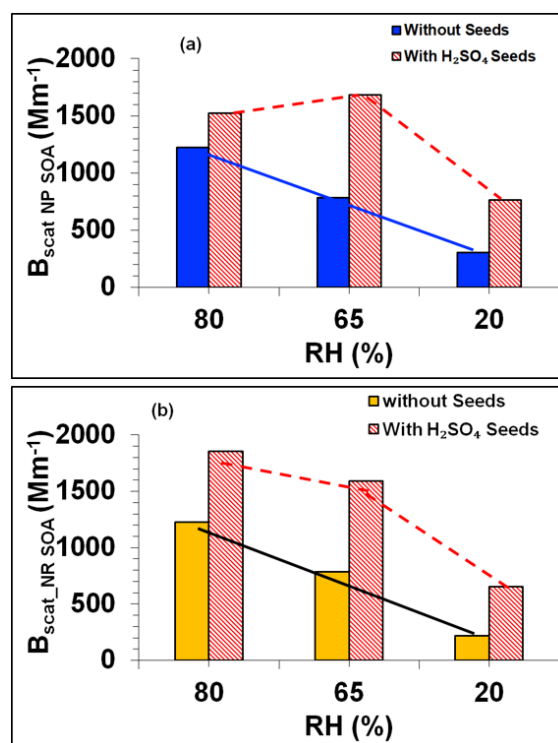


Figure 15. (a,b): Effects of water vapour and acidity on the B_{scat} of toluene SOA. (a) B_{scat} of NP SOA for the H₂SO₄ seeded and non-seeded experiments at the three RHs; (b) B_{scat} of NR SOA for the H₂SO₄ seeded and non-seeded experiments at the three RHs. The solid and dashed lines are eye guides.

4. Conclusions

We observed that the pattern of SOA mass formation at $[\text{NO}_x]/[\Delta\text{HC}]$ molar ratios below 0.15 differed markedly from that seen at higher $[\text{NO}_x]/[\Delta\text{HC}]$ ratios. We therefore distinguish between nitrogen-poor (NP) SOA formed under conditions with low initial NO_x concentrations and nitrogen-rich (NR) SOA, which has a higher content of compounds such as organo-nitrates. We suggest that this distinction is valuable for understanding trends in the formation and properties of SOA formation in the presence of varying concentrations of NO_x . The SOA mass generally decreased as the $[\text{NO}_x]/[\Delta\text{HC}]$ ratio increased, especially under the NR regime of our proposed framework. In addition, NO_x promoted SOA browning under both regimes.

Under the NP regime, MAC increased with $[\text{NO}_x]/[\Delta\text{HC}]$ independently of the RH. However, for NR SOA, the MAC depended significantly on both $[\text{NO}_x]/[\Delta\text{HC}]$ and the RH. The RH also had a complex effect on SOA browning (measured in terms of the MAC) under NR conditions but did not promote browning under NP conditions. The mass scattering cross-section (MSC, defined as $B_{\text{scat}}/[\text{SOA Mass}]$) of NR SOA also depended on the RH (and by extension, on OH exposure): it increased with $[\text{NO}_x]/[\Delta\text{HC}]$ at RH values above 65% but decreased as $[\text{NO}_x]/[\Delta\text{HC}]$ increased at RH values below 35%.

Both B_{abs} and MAC increased with the $[\text{NH}_3]/[\Delta\text{HC}]$ ratio, suggesting that NH_3 promotes the formation of N-H-containing organic chromophores such as cyclic amines and azo compounds with similar peak B_{abs} values under low NO_x conditions. In addition, the formation of ammonium nitrate was observed in toluene- NH_3 -OH systems at low NO_x concentrations. NH_3 had no strong effect on SOA mass formation under high NO_x conditions but when the NO_x concentration was low, NH_3 significantly increased both the mass of SOA that formed and its light absorbing and scattering capacity. In addition, under high NO_x conditions, the presence of NH_3 increased the MAC and MSC when compared to the case without NH_3 .

Acidity strongly promoted SOA mass formation. The SOA mass enhancement due to acidity was highest (30% and 21% in the NR and NP SOA, respectively) at the lowest RH (20%); under higher pH conditions with 65% RH, acidity had no appreciable effect on SOA mass formation. Moreover, at 80%, when the pH was highest, H_2SO_4 seeding reduced SOA mass formation by 35% and 21% in the NP and NR regimes, respectively. These results show that acidity has complex effects on SOA mass formation that depend on both the NO_x concentration and the RH.

The MAC was significantly enhanced in both NP and NR regimes in the H_2SO_4 seeded SOA, indicating that acidity plays an important role in SOA browning. In addition, the MACs of the H_2SO_4 -seeded SOA were higher at intermediate and low RH than at high RH (80%). This finding was rationalized by suggesting that the MAC enhancement of acidic SOA is linked to the formation of organosulphate chromophores and governed by two major parameters: the pH of the SOA aqueous phase and the ratio of the free hydrogen ion concentration in the aqueous phase ($[\text{H}^+]_{\text{free}}$) to the SOA mass.

Acid seeding also increased the B_{scat} of the SOA, which can be attributed to increases in the surface area and scattering potential of the SOA caused by the sulfuric acid seeds. There was no clear evidence that acid seeding or variation in the RH changed the chemical composition of the SOA in ways that greatly affected B_{scat} ; however, instead, the changes in B_{scat} and MSC in seeded SOA under NP and NR conditions are primarily attributed to increased surface growth driven by H_2SO_4 seeds.

Incorporating these findings into climate and air quality models will reduce uncertainties in the treatment of SOA and a deeper understanding of its role in climate change.

Supplementary Materials: The following supporting information can be downloaded at <https://www.mdpi.com/article/10.3390/atmos13071099/s1>. Table S1: The estimated total OH concentration exposure (OH exp) and equivalent atmospheric aging (*Hrs and Days*) of SOA in GO:PAM. Table S2: NR Regime ($\text{NO}_x/\Delta\text{HC} > 0.15$) SOA properties and parameterization. Table S3: E-AIM model results and pH for $22.3 \mu\text{g m}^{-3}$ dried H_2SO_4 injected in each experiment. Figure S1: Process flow

diagram of the experimental setup. Figure S2: SOA mass as a function of RH in the NP and NR SOA formation regimes. Figure S3: Mass enhancement factor (MEF) as a function of relative humidity for toluene-OH photo-oxidation SOA. A fit to data reported by Liu et al. [33] is plotted alongside a fit to data originating from this work for toluene SOAs formed at different RH values and NO_x concentrations. The MEF in this study was estimated based on the SOA mass at 20% RH with the assumption that the hygroscopic growth factor for SOA at 20% RH relative to that at around 0% RH is approximately 1.03, as reported by Liu et al. [33]. Figure S4: B_{scat} as a function of RH in the NP and NR SOA formation regimes. NP and NR results are plotted using empty blue and filled red circles, respectively. Figure S5: Aerosol liquid water (ALW) content as a function of RH in the NP and NR regimes of SOA formation. NP and NR results are plotted using empty blue and filled red circles, respectively. Figure S6: MSC as a function of RH in the NP and NR SOA formation regimes. NP and NR results are plotted using empty blue and filled red circles, respectively. Best fits for NP and NR are shown using solid blue and dotted red lines, respectively. Figure S7: Single Scattering Albedo (SSA) as a function of the NO_x to reacted toluene ratio ($[\text{NO}_x]/[\Delta\text{HC}]$) at 80% RH, 65% RH, 35% RH, and 20% RH. Empty and filled symbols show results for nitrogen poor (NP) and nitrogen rich (NR) SOA, respectively. The blue solid line is the trend line for NP SOA. Figure S8: SSA as a function of RH in the NP and NR SOA formation regimes. NP and NR results are plotted using empty blue and filled red circles, respectively. Best fit lines for NP and NR are solid blue and dotted red, respectively. Figure S9: (a,b): Effect of NH_3 on the light scattering properties of SOA at 80% RH under low and high NO_x conditions. (a) B_{scat} as a function of the ($[\text{NH}_3]/[\Delta\text{HC}]$) ratio; (b) MSC as a function of the ($[\text{NH}_3]/[\Delta\text{HC}]$) ratio. Figure S10: (a–f): Effects of acidity and RH on SOA mass, ALW, and pH for NP and NR SOA: (a) NP SOA mass as a function of RH in the H_2SO_4 seeded and non-seeded experiments; (b) NR SOA mass as a function of RH in the H_2SO_4 seeded and non-seeded experiments; (c) NP and NR SOA mass as functions of the RH in the H_2SO_4 seeded experiments; (d) ALW in NP SOA as a function of RH in the H_2SO_4 seeded and non-seeded experiments; (e) ALW in NR SOA as a function of RH in the H_2SO_4 seeded and non-seeded experiments; (f) pH of the NP and NR SOA as functions of the RH in the H_2SO_4 seeded experiments. Non-seeded experiments are Tol-1, Tol-2 and Tol-4, while H_2SO_4 seeded experiments are Tol-7, Tol-8 and Tol-9. Figure S11: (a–f): Effects of acidity, NO_x , and RH on the B_{scat} and MSC of toluene SOA. (i) B_{scat} as a function of $[\text{NO}_x]/[\Delta\text{HC}]$ for the H_2SO_4 seeded and non-seeded experiments at (a) 80%, (b) 65%, and (c) 20% RH. (ii) MSC as a function of $[\text{NO}_x]/[\Delta\text{HC}]$ for the H_2SO_4 seeded and non-seeded experiments at (d) 80%, (e) 65%, and (f) 20% RH. Solid lines in (a), (b), and (c) are eye guides showing trends in B_{scat} for NP and NR SOA in the non-seeded case, while the dotted lines show trends for NP and NR SOA in the H_2SO_4 -seeded SOA experiments. In (d–f) the solid lines are eye guides for the NP and NR SOA cases in the H_2SO_4 seeded experiments while the dotted lines are eye guides for NP and NR SOA in the non-seeded experiments. Figure S12: (a,b): Effects of water vapor and acidity on the MSC of toluene SOA. (a) MSC of NP SOA for the H_2SO_4 seeded and non-seeded experiments at three RHs; (b) MSC of NR SOA for the H_2SO_4 seeded and non-seeded experiments at the three RHs. Figure S13: An example time series of experimental results.

Author Contributions: Conceptualization, R.K.P.; methodology, R.K.P., K.M., X.P. and H.R.M.; software, K.M. and R.K.P.; validation, K.M., H.R.M. and R.K.P.; formal analysis, K.M., H.R.M. and R.K.P.; investigation, K.M., X.P. and R.K.P.; resources, R.K.P. and K.M.; data curation, K.M., H.R.M. and R.K.P.; writing—original draft preparation, K.M. and R.K.P.; writing—review and editing, K.M., H.R.M., X.P. and R.K.P.; visualization, K.M. and R.K.P.; supervision, R.K.P.; project administration, R.K.P. and K.M.; funding acquisition, R.K.P. All authors have read and agreed to the published version of the manuscript.

Funding: This research was funded by Vetenskapsrådet (Swedish Research Council, VR) under grant 2015-04123 and The RKP was funded by Vetenskapsrådet, Sweden.

Institutional Review Board Statement: Not applicable.

Informed Consent Statement: Not applicable.

Data Availability Statement: The data reported in this study are available within the manuscript and in Supplementary Materials. We will also publish at least one follow-up companion article with m/z values in this journal, along with that we will put all associated raw data to our university's open access server.

Acknowledgments: We acknowledge support from Mattias Hallquist for providing the CIMS machine and Christian Mark Salvador for operating the CIMS machine.

Conflicts of Interest: The authors declare no conflict of interest. The funders had no role in the design of the study; in the collection, analyses, or interpretation of data; in the writing of the manuscript; or in the decision to publish the results.

References

1. Arias, P.A.; Bellouin, N.; Coppola, E.; Jones, R.G.; Krinner, G.; Marotzke, J.; Naik, V.; Palmer, M.D.; Plattner, G.; Rogelj, J.; et al. IPCC, 2021: Technical Summary. In *Climate Change 2021: The Physical Science Basis. Contribution of Working Group 15 I to the Sixth Assessment Report of the Intergovernmental Panel on Climate Change*; Masson-Delmotte, V., Zhai, P., Pirani, A., Connors, S.L., Péan, C., Berger, S., Caud, N., Chen, Y., Goldfarb, L., Gomis, M.I., et al., Eds.; IPCC AR6 WGI; Cambridge University Press: Cambridge, UK, 2021; pp. 1–3949, *in press*.
2. Kanakidou, M.; Seinfeld, J.H.; Pandis, S.N.; Barnes, I.; Dentener, F.J.; Facchini, M.C.; Van Dingenen, R.; Ervens, B.; Nenes, A.; Nielsen, C.J.; et al. Organic aerosol and global climate modelling: A review. *Atmos. Chem. Phys.* **2005**, *5*, 1053–1123. [[CrossRef](#)]
3. Hallquist, M.; Wenger, J.C.; Baltensperger, U.; Rudich, Y.; Simpson, D.; Claeys, M.; Dommen, J.; Donahue, N.M.; George, C.; Goldstein, A.H.; et al. The formation, properties and impact of secondary organic aerosol: Current and emerging issues. *Atmos. Chem. Phys.* **2009**, *9*, 5155–5236. [[CrossRef](#)]
4. Myhre, G.; Samset, B.H.; Schulz, M.; Balkanski, Y.; Bauer, S.; Bernsten, T.K.; Bian, H.; Bellouin, N.; Chin, M.; Diehl, T.; et al. Radiative forcing of the direct aerosol effect from AeroCom Phase II simulations. *Atmos. Chem. Phys.* **2013**, *13*, 1853–1877. [[CrossRef](#)]
5. Ervens, B.; Turpin, B.J.; Weber, R.J. Secondary organic aerosol formation in cloud droplets and aqueous particles (aqSOA): A review of laboratory, field and model studies. *Atmos. Chem. Phys.* **2011**, *11*, 11069–11102. [[CrossRef](#)]
6. Herckes, P.; Lee, T.; Trenary, L.; Kang, G.G.; Chang, H.; Collett, J.L. Organic matter in Central California radiation fogs. *Environ. Sci. Technol.* **2002**, *36*, 4777–4782. [[CrossRef](#)]
7. Carlton, A.G.; Wiedinmyer, C.; Kroll, J.H. A review of Secondary Organic Aerosol (SOA) formation from isoprene. *Atmos. Chem. Phys.* **2009**, *9*, 4987–5005. [[CrossRef](#)]
8. Kroll, J.H.; Seinfeld, J.H. Chemistry of secondary organic aerosol: Formation and evolution of low-volatility organics in the atmosphere. *Atmos. Environ.* **2008**, *42*, 3593–3624. [[CrossRef](#)]
9. Rudich, Y.; Donahue, N.M.; Mentel, T.F. Aging of organic aerosol: Bridging the gap between laboratory and field studies. *Annu. Rev. Phys. Chem.* **2007**, *58*, 321–352. [[CrossRef](#)]
10. Kalberer, M.; Paulsen, D.; Sax, M.; Steinbacher, M.; Dommen, J.; Prevot, A.S.H.; Fisseha, R.; Weingartner, E.; Frankevich, V.; Zenobi, R.; et al. Identification of polymers as major components of atmospheric organic aerosols. *Science* **2004**, *303*, 1659–1662. [[CrossRef](#)] [[PubMed](#)]
11. Ehn, M.; Kleist, E.; Junninen, H.; Petaja, T.; Lonn, G.; Schobesberger, S.; Dal Maso, M.; Trimborn, A.; Kulmala, M.; Worsnop, D.R.; et al. Gas phase formation of extremely oxidized pinene reaction products in chamber and ambient air. *Atmos. Chem. Phys.* **2012**, *12*, 5113–5127. [[CrossRef](#)]
12. Laskin, J.; Laskin, A.; Nizkorodov, S.A.; Roach, P.; Eckert, P.; Gilles, M.K.; Wang, B.B.; Lee, H.J.; Hu, Q.C. Molecular Selectivity of Brown Carbon Chromophores. *Environ. Sci. Technol.* **2014**, *48*, 12047–12055. [[CrossRef](#)] [[PubMed](#)]
13. Laskin, A.; Laskin, J.; Nizkorodov, S.A. Chemistry of Atmospheric Brown Carbon. *Chem. Rev.* **2015**, *115*, 4335–4382. [[CrossRef](#)] [[PubMed](#)]
14. Saleh, R.; Hennigan, C.J.; McMeeking, G.R.; Chuang, W.K.; Robinson, E.S.; Coe, H.; Donahue, N.M.; Robinson, A.L. Absorptivity of brown carbon in fresh and photo-chemically aged biomass-burning emissions. *Atmos. Chem. Phys.* **2013**, *13*, 7683–7693. [[CrossRef](#)]
15. Zhong, M.; Jang, M. Dynamic light absorption of biomass-burning organic carbon photochemically aged under natural sunlight. *Atmos. Chem. Phys.* **2014**, *14*, 1517–1525. [[CrossRef](#)]
16. Bond, T.C. Spectral dependence of visible light absorption by carbonaceous particles emitted from coal combustion. *Geophys. Res. Lett.* **2001**, *28*, 4075–4078. [[CrossRef](#)]
17. Kirchstetter, T.W.; Novakov, T.; Hobbs, P.V. Evidence that the spectral dependence of light absorption by aerosols is affected by organic carbon. *J. Geophys. Res. Atmos.* **2004**, *109*, 12. [[CrossRef](#)]
18. Lack, D.A.; Langridge, J.M.; Bahreini, R.; Cappa, C.D.; Middlebrook, A.M.; Schwarz, J.P. Brown carbon and internal mixing in biomass burning particles. *Proc. Natl. Acad. Sci. USA* **2012**, *109*, 14802–14807. [[CrossRef](#)]
19. Andreae, M.O.; Crutzen, P.J. Atmospheric aerosols: Biogeochemical sources and role in atmospheric chemistry. *Science* **1997**, *276*, 1052–1058. [[CrossRef](#)]
20. Ng, N.L.; Kroll, J.H.; Chan, A.W.H.; Chhabra, P.S.; Flagan, R.C.; Seinfeld, J.H. Secondary organic aerosol formation from m-xylene, toluene, and benzene. *Atmos. Chem. Phys.* **2007**, *7*, 3909–3922. [[CrossRef](#)]
21. Odum, J.R.; Jungkamp, T.P.W.; Griffin, R.J.; Flagan, R.C.; Seinfeld, J.H. The atmospheric aerosol-forming potential of whole gasoline vapor. *Science* **1997**, *276*, 96–99. [[CrossRef](#)]

22. Odum, J.R.; Jungkamp, T.P.W.; Griffin, R.J.; Forstner, H.J.L.; Flagan, R.C.; Seinfeld, J.H. Aromatics, reformulated gasoline, and atmospheric organic aerosol formation. *Environ. Sci. Technol.* **1997**, *31*, 1890–1897. [[CrossRef](#)]
23. Zhang, R.Y.; Wang, G.H.; Guo, S.; Zarnora, M.L.; Ying, Q.; Lin, Y.; Wang, W.G.; Hu, M.; Wang, Y. Formation of Urban Fine Particulate Matter. *Chem. Rev.* **2015**, *115*, 3803–3855. [[CrossRef](#)] [[PubMed](#)]
24. Hildebrandt, L.; Donahue, N.M.; Pandis, S.N. High formation of secondary organic aerosol from the photo-oxidation of toluene. *Atmos. Chem. Phys.* **2009**, *9*, 2973–2986. [[CrossRef](#)]
25. Odum, J.R.; Hoffmann, T.; Bowman, F.; Collins, D.; Flagan, R.C.; Seinfeld, J.H. Gas/particle partitioning and secondary organic aerosol yields. *Environ. Sci. Technol.* **1996**, *30*, 2580–2585. [[CrossRef](#)]
26. Lin, P.; Liu, J.M.; Shilling, J.E.; Kathmann, S.M.; Laskin, J.; Laskin, A. Molecular characterization of brown carbon (BrC) chromophores in secondary organic aerosol generated from photo-oxidation of toluene. *Phys. Chem. Chem. Phys.* **2015**, *17*, 23312–23325. [[CrossRef](#)]
27. Liu, J.M.; Lin, P.; Laskin, A.; Laskin, J.; Kathmann, S.M.; Wise, M.; Caylor, R.; Imholt, F.; Selimovic, V.; Shilling, J.E. Optical properties and aging of light-absorbing secondary organic aerosol. *Atmos. Chem. Phys.* **2016**, *16*, 12815–12827. [[CrossRef](#)]
28. Zhang, W.Y.; Wang, W.G.; Li, J.L.; Peng, C.; Li, K.; Zhou, L.; Shi, B.; Chen, Y.; Liu, M.Y.; Ge, M.F. Effects of SO₂ on optical properties of secondary organic aerosol generated from photooxidation of toluene under different relative humidity conditions. *Atmos. Chem. Phys.* **2020**, *20*, 4477–4492. [[CrossRef](#)]
29. Li, K.; Wang, W.G.; Ge, M.F.; Li, J.J.; Wang, D. Optical properties of secondary organic aerosols generated by photooxidation of aromatic hydrocarbons. *Sci. Rep.* **2014**, *4*, 9. [[CrossRef](#)]
30. Kim, H.; Paulson, S.E. Real refractive indices and volatility of secondary organic aerosol generated from photooxidation and ozonolysis of limonene, alpha-pinene and toluene. *Atmos. Chem. Phys.* **2013**, *13*, 7711–7723. [[CrossRef](#)]
31. Moise, T.; Flores, J.M.; Rudich, Y. Optical Properties of Secondary Organic Aerosols and Their Changes by Chemical Processes. *Chem. Rev.* **2015**, *115*, 4400–4439. [[CrossRef](#)]
32. Nakayama, T.; Sato, K.; Matsumi, Y.; Imamura, T.; Yamazaki, A.; Uchiyama, A. Wavelength and NO_x dependent complex refractive index of SOAs generated from the photooxidation of toluene. *Atmos. Chem. Phys.* **2013**, *13*, 531–545. [[CrossRef](#)]
33. Liu, P.F.; Song, M.J.; Zhao, T.N.; Gunthe, S.S.; Ham, S.H.; He, Y.P.; Qin, Y.M.; Gong, Z.H.; Amorim, J.C.; Bertram, A.K.; et al. Resolving the mechanisms of hygroscopic growth and cloud condensation nuclei activity for organic particulate matter. *Nat. Commun.* **2018**, *9*, 10. [[CrossRef](#)] [[PubMed](#)]
34. Liu, T.Y.; Huang, D.D.; Li, Z.J.; Liu, Q.Y.; Chan, M.N.; Chan, C.K. Comparison of secondary organic aerosol formation from toluene on initially wet and dry ammonium sulfate particles at moderate relative humidity. *Atmos. Chem. Phys.* **2018**, *18*, 5677–5689. [[CrossRef](#)]
35. Tsiligiannis, E.; Hammes, J.; Salvador, C.M.; Mentel, T.F.; Hallquist, M. Effect of NO_x on 1,3,5-trimethylbenzene (TMB) oxidation product distribution and particle formation. *Atmos. Chem. Phys.* **2019**, *19*, 15073–15086. [[CrossRef](#)]
36. Backstrom, D.; Gunnarsson, A.; Gall, D.; Pei, X.Y.; Johansson, R.; Andersson, K.; Pathak, R.K.; Pettersson, J.B.C. Measurement of the size distribution, volume fraction and optical properties of soot in an 80 kW propane flame. *Combust. Flame* **2017**, *186*, 325–334. [[CrossRef](#)]
37. Lopez-Hilfiker, F.D.; Mohr, C.; Ehn, M.; Rubach, F.; Kleist, E.; Wildt, J.; Mentel, T.F.; Lutz, A.; Hallquist, M.; Worsnop, D.; et al. A novel method for online analysis of gas and particle composition: Description and evaluation of a Filter Inlet for Gases and AEROSols (FIGAERO). *Atmos. Meas. Tech.* **2014**, *7*, 983–1001. [[CrossRef](#)]
38. Aljawhary, D.; Lee, A.K.Y.; Abbatt, J.P.D. High-resolution chemical ionization mass spectrometry (ToF-CIMS): Application to study SOA composition and processing. *Atmos. Meas. Tech.* **2013**, *6*, 3211–3224. [[CrossRef](#)]
39. Ziemann, P.J.; Atkinson, R. Kinetics, products, and mechanisms of secondary organic aerosol formation. *Chem. Soc. Rev.* **2012**, *41*, 6582–6605. [[CrossRef](#)]
40. Jimenez, P.J.-L. *Laboratory Experiments and Modeling for Interpreting Field Studies of Secondary Organic Aerosol Formation Using an Oxidation Flow Reactor*; DOE/SC0006035-1; The U.S. Department OF Energy Office of Science Office of Biological and Environmental Research Atmospheric Systems Research Program under Contract NO. DE-SC0006035: Boulder, CO, USA, 2016; pp. 1–46.
41. Mao, J.; Ren, X.; Brune, W.H.; Olson, J.R.; Crawford, J.H.; Fried, A.; Huey, L.G.; Cohen, R.C.; Heikes, B.; Singh, H.B.; et al. Airborne measurement of OH reactivity during INTEX-B. *Atmos. Chem. Phys.* **2009**, *9*, 163–173. [[CrossRef](#)]
42. DMT. *Three-Wavelength Photoacoustic Soot Spectrometer (PASS-3) Operator Manual*; DOC-0163 Revision D; Droplet Measurement Technologies, Inc.: Boulder, CO, USA, 2011.
43. Atkinson, R.; Aschmann, S.M. Rate Constants for the Gas-Phase Reactions of the Oh Radical with a Series of Aromatic-Hydrocarbons at 296+/-2-K. *Int. J. Chem. Kinet.* **1989**, *21*, 355–365. [[CrossRef](#)]
44. Simon, L.; Clegg, P.B.; Anthony, S.W. Extended AIM Aerosol Thermodynamics Model. Available online: <http://www.aim.env.uea.ac.uk/aim/aim.php> (accessed on 8 March 2022).
45. Presto, A.A.; Hartz, K.E.H.; Donahue, N.M. Secondary organic aerosol production from terpene ozonolysis. 2. Effect of NO_x concentration. *Environ. Sci. Technol.* **2005**, *39*, 7046–7054. [[CrossRef](#)] [[PubMed](#)]
46. Takeuchi, M.; Ng, N.L. Organic Nitrates and Secondary Organic Aerosol (SOA) Formation from Oxidation of Biogenic Volatile Organic Compounds. In *Multiphase Environmental Chemistry in the Atmosphere*; ACS Symposium Series; American Chemical Society: Washington, DC, USA, 2018; Volume 1299, pp. 105–125.

47. Qi, X.; Zhu, S.P.; Zhu, C.Z.; Hu, J.; Lou, S.R.; Xu, L.; Dong, J.G.; Cheng, P. Smog chamber study of the effects of NO_x and NH₃ on the formation of secondary organic aerosols and optical properties from photo-oxidation of toluene. *Sci. Total Environ.* **2020**, *727*, 10. [[CrossRef](#)] [[PubMed](#)]
48. Chen, L.H.; Bao, Z.E.; Wu, X.C.; Li, K.W.; Han, L.X.; Zhao, X.Y.; Zhang, X.; Wang, Z.H.; Azzi, M.; Cen, K.F. The effects of humidity and ammonia on the chemical composition of secondary aerosols from toluene/NO_x photo-oxidation. *Sci. Total Environ.* **2020**, *728*, 10. [[CrossRef](#)]
49. Bao, Z.E.; Xu, H.F.; Li, K.W.; Chen, L.H.; Zhang, X.; Wu, X.C.; Gao, X.; Azzi, M.; Cen, K.F. Effects of NH₃ on secondary aerosol formation from toluene/NO_x photo-oxidation in different O₃ formation regimes. *Atmos. Environ.* **2021**, *261*, 11. [[CrossRef](#)]
50. Jang, M.S.; Czoschke, N.M.; Lee, S.; Kamens, R.M. Heterogeneous atmospheric aerosol production by acid-catalyzed particle-phase reactions. *Science* **2002**, *298*, 814–817. [[CrossRef](#)] [[PubMed](#)]
51. Deng, Y.G.; Inomata, S.; Sato, K.; Ramasamy, S.; Morino, Y.; Enami, S.; Tanimoto, H. Temperature and acidity dependence of secondary organic aerosol formation from alpha-pinene ozonolysis with a compact chamber system. *Atmos. Chem. Phys.* **2021**, *21*, 5983–6003. [[CrossRef](#)]
52. Cao, G.; Jang, M. Secondary organic aerosol formation from toluene photooxidation under various NO_x conditions and particle acidity. *Atmos. Chem. Phys. Discuss.* **2008**, *2008*, 14467–14495. [[CrossRef](#)]
53. McNeill, V.F.; Woo, J.L.; Kim, D.D.; Schwiier, A.N.; Wannell, N.J.; Sumner, A.J.; Barakat, J.M. Aqueous-Phase Secondary Organic Aerosol and Organosulfate Formation in Atmospheric Aerosols: A Modeling Study. *Environ. Sci. Technol.* **2012**, *46*, 8075–8081. [[CrossRef](#)]